

2

DTIC FILE COPY

NAVAL POSTGRADUATE SCHOOL Monterey, California

AD-A222 806



THESIS

DTIC
SELECTE
JUN 19 1990
S E D

CLOUD REFLECTANCE CHARACTERISTICS IN
THE PRESENCE
OF VARIABLE DIMETHYLSULFIDE (DMS)
SOURCES

by

Greg A. Eisman

September 1989

Thesis Advisor

Philip A. Durkee

Approved for public release; distribution is unlimited.

Color and resolution color
plates: All data reproductions
will be in black and
white.

Unclassified

security classification of this page

REPORT DOCUMENTATION PAGE

1a Report Security Classification Unclassified		1b Restrictive Markings	
2a Security Classification Authority		3 Distribution Availability of Report Approved for public release; distribution is unlimited.	
2b Declassification Downgrading Schedule			
4 Performing Organization Report Number(s)		5 Monitoring Organization Report Number(s)	
6a Name of Performing Organization Naval Postgraduate School	6b Office Symbol <i>(if applicable)</i> 35	7a Name of Monitoring Organization Naval Postgraduate School	
6c Address (city, state, and ZIP code) Monterey, CA 93943-5000		7b Address (city, state, and ZIP code) Monterey, CA 93943-5000	
8a Name of Funding Sponsoring Organization	8b Office Symbol <i>(if applicable)</i>	9 Procurement Instrument Identification Number	
8c Address (city, state, and ZIP code)		10 Source of Funding Numbers	
		Program Element No	Project No
		Task No	Work Unit Accession No
11 Title (include security classification) CLOUD REFLECTANCE CHARACTERISTICS IN THE PRESENCE OF VARIABLE DIMETHYLSULFIDE (DMS) SOURCES			
12 Personal Author(s) Greg A. Eisman			
13a Type of Report Master's Thesis	13b Time Covered From To	14 Date of Report (year, month, day) September 1989	15 Page Count 52
16 Supplementary Notation The views expressed in this thesis are those of the author and do not reflect the official policy or position of the Department of Defense or the U.S. Government.			
17 Cosatt Codes		18 Subject Terms (continue on reverse if necessary and identify by block number)	
Field	Group	Subgroup	DMS, silicon anomaly, AVHRR satellite imagery (T ES) ← at atmospheric physics,
19 Abstract (continue on reverse if necessary and identify by block number)			
<p>Oceanic dimethylsulfide (DMS) sources are inferred from silicon anomaly information in the Denmark Strait during June 1984. This June 1984 "bloom" of the phytoplankton species <i>Phaeocystes pouchetti</i>, a known DMS producer, is compared to the "non-bloom" of June 1982 using NOAA-7 AVHRR data from channel 1 (0.63 μm), channel 3 (3.7 μm) and channel 4 (11.0 μm) wavelengths. After examining the AVHRR color-enhanced data for each individual day, composites for June 1982 and June 1984 are created for channel 1 and channel 3 wavelengths. These composites eliminated day-to-day differences in reflectances by averaging data which were neither cloud-free nor high-cloud contaminated. Based on these composites, evidence is presented which suggests that a correlation exists between inferred-DMS source regions and higher reflectance values at channel 3 wavelengths.</p> <p style="text-align: right;">→ MICRONS</p>			
20 Distribution Availability of Abstract <input checked="" type="checkbox"/> unclassified unlimited <input type="checkbox"/> same as report <input type="checkbox"/> DTIC users		21 Abstract Security Classification Unclassified	
22a Name of Responsible Individual Philip A. Durkee		22b Telephone (include Area code) (408) 646-2044	22c Office Symbol 631De

Approved for public release; distribution is unlimited.

Cloud Reflectance Characteristics in the Presence
of Variable Dimethylsulfide (DMS) Sources

by

Greg A. Eisman
Lieutenant, United States Navy
B.S., United States Naval Academy, 1982

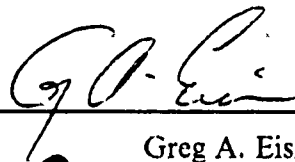
Submitted in partial fulfillment of the
requirements for the degree of

MASTER OF SCIENCE IN METEOROLOGY AND OCEANOGRAPHY

from the

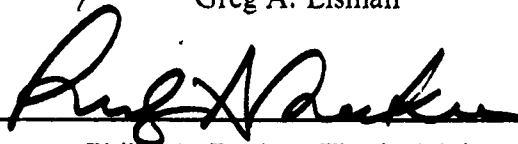
NAVAL POSTGRADUATE SCHOOL
September 1989

Author:

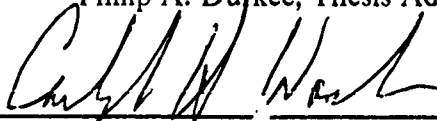


Greg A. Eisman

Approved by:



Philip A. Durkee, Thesis Advisor



Carlyle H. Wash, Second Reader



Robert J. Renard, Chairman,
Department of Meteorology

ABSTRACT

Oceanic dimethylsulfide (DMS) sources are inferred from silicon anomaly information in the Denmark Strait during June 1984. This June 1984 "bloom" of the phytoplankton species *Phaecystes pouchetti*, a known DMS producer, is compared to the "non-bloom" of June 1982 using NOAA-7 AVHRR data from channel 1 ($0.63 \mu m$), channel 3 ($3.7 \mu m$) and channel 4 ($11.0 \mu m$) wavelengths. After examining the AVHRR color-enhanced data for each individual day, composites for June 1982 and June 1984 are created for channel 1 and channel 3 wavelengths. These composites eliminated day-to-day differences in reflectances by averaging data which were neither cloud-free nor high-cloud contaminated. Based on these composites, evidence is presented which suggests that a correlation exists between inferred-DMS source regions and higher reflectance values at channel 3 wavelengths.

Accession For	
NTIS GRA&I	<input checked="" type="checkbox"/>
DTIC TAB	<input type="checkbox"/>
Unannounced	<input type="checkbox"/>
Justification	
By _____	
Distribution/	
Availability Codes	
Dist	Avail and/or Special
A-1	



"Original contains color
plates: All DTIC reproductions
will be in black and
white"

TABLE OF CONTENTS

I. INTRODUCTION	1
A. RADIATIVE PROCESSES	2
B. MOTIVATION	5
C. OBJECTIVES	9
II. DATA ANALYSIS	10
A. DATA ACQUISITION/DESCRIPTION	10
B. DATA PROCESSING	10
1. Channel 1.	11
2. Channel 3	11
3. Channel 4	11
4. Composite Images	14
III. RESULTS	16
A. CASE 1. SAMPLE 1982 DATA SET	16
1. Synoptic Overview for June 1982	16
2. AVHRR Analysis for 12 June 1982 (Case 1A)	16
3. AVHRR Analysis for 13 June 1982 (Case 1B)	17
B. CASE 2. SAMPLE 1984 DATA SET	21
1. Synoptic Overview for 1800 UTC on 13 June 1984	21
2. AVHRR Analysis for 9 June 1984 (Case 2A)	21
3. AVHRR Analysis for 13 June 1984 (Case 2B)	25
C. COMPOSITE RESULTS	29
D. SECTOR RESULTS	37
IV. CONCLUSIONS AND RECOMMENDATIONS	40
A. CONCLUSIONS	40
B. RECOMMENDATIONS	41
LIST OF REFERENCES	42

INITIAL DISTRIBUTION LIST 43

LIST OF FIGURES

Fig. 1. Conceptual Diagram of Possible Climate Feedback Loop.	3
Fig. 2. Schematic of visible (.63 μm) and near-IR (3.7 μm) energy interactions with clouds.	5
Fig. 3. Channel 1 (.63 μm) and channel 3 (3.7 μm) reflectance versus mean droplet radius, from Mineart (1988).	6
Fig. 4. Map showing Denmark Strait and the study analysis region.	7
Fig. 5. Silicate anomalies ($\mu\text{mol/L}$) in the Spring of 1984 near Iceland, from Olafsson, 1988 (personal communication).	8
Fig. 6. Silicate anomalies ($\mu\text{mol/L}$) in the Spring of 1982 near Iceland, from Olafsson, 1988 (personal communication).	8
Fig. 7. LOW1 (AVHRR channel 1, low-cloud anisotropy corrected) image at 1415 UTC on 12 June 1982.	12
Fig. 8. LOW3 (AVHRR channel 3, low-cloud anisotropy corrected) image at 1415 UTC on 12 June 1982.	13
Fig. 9. Flowchart illustrating composite averaging algorithm.	15
Fig. 10. Mean sea-level pressure analysis and plotted surface data for 1200 UTC on 12 June 1982.	17
Fig. 11. LOW1 image for 1415 UTC on 12 June 1982.	18
Fig. 12. LOW3 image for 1415 UTC on 12 June 1982.	19
Fig. 13. TEMP4 image for 1415 UTC on 12 June 1982.	20
Fig. 14. LOW1 image at 1403 UTC on 13 June 1982.	22
Fig. 15. LOW3 image at 1403 UTC on 13 June 1982.	23
Fig. 16. TEMP4 image at 1403 UTC on 13 June 1982.	24
Fig. 17. Mean sea-level pressure analysis and plotted surface data for 0941 UTC on 13 June 1984.	25
Fig. 18. LOW1 image for 0941 UTC on 9 June 1984.	26
Fig. 19. LOW3 image for 0941 UTC on 9 June 1984.	27
Fig. 20. TEMP4 image for 0941 UTC on 9 June 1984.	28
Fig. 21. LOW1 image for 1655 UTC on 13 June 1984.	30
Fig. 22. LOW3 image for 1655 UTC on 13 June 1984.	31
Fig. 23. TEMP4 image for 1655 UTC on 13 June 1984.	32

Fig. 24. LOW1 composite for June 1982.	33
Fig. 25. LOW1 composite for June 1984.	34
Fig. 26. LOW3 composite for June 1982.	35
Fig. 27. LOW3 composite for June 1984.	36
Fig. 28. Location of the eight sectors around Iceland.	39

ACKNOWLEDGMENTS

I would like to thank Professor Philip A. Durkee for his assistance, guidance and support throughout the course of this research. A special thanks to Professor Carlyle H. Wash for his careful review of this work. In addition, the staff of the Naval Post-graduate School's Interactive Digital Environmental Analysis (IDEA) Laboratory is commended for their support, especially Mr. Craig E. Motell. Without his programming skills this project could not have been completed. Finally, a loving thanks to my wife Susan and daughter Amanda, whose emotional support and unending patience were priceless throughout this endeavor.

I. INTRODUCTION

Global climate processes have been studied in great detail in recent years. Various hypotheses have been proposed describing both global warming and cooling trends. The "greenhouse effect, absorption by the atmosphere of infrared (IR) energy emitted from the earth, has been regarded as a prominent theory for producing a global warming trend. In addition, deforestation, urban carbon dioxide (CO_2) production and volcanic eruptions have been proposed as planetary sources of warming/cooling. Other studies indicate a general cooling trend due to increases in small aerosol particles in the atmosphere. Twomey et al.(1984) suggests that increased pollution may have such an effect. The increase in aerosol concentration increases the number of cloud condensation nuclei (CCN). This increase in CCN increases the number of cloud droplets, and assuming constant liquid water content (LWC), decreases the droplet radius. The result is more reflection of short-wave radiation, hence lower overall surface temperatures. However, at the same time some clouds, especially high cirrus clouds, have the ability to increase absorption of outgoing long-wave radiation, thereby warming the earth. Thus, an important dichotomy exists; clouds both reflect incoming short-wave radiation (a cooling effect) and absorb outgoing long-wave radiation (a warming effect). General circulation models (GCM's) have a tendency to neglect or over-simplify clouds due to their extreme complexity and spatial variability. Nonetheless, these factors influencing variations in global mean temperature illustrate the diversified, intricate environmental processes which control climate.

One important process affecting climate on a global scale has been hypothesized by Charlson et al.(1987). He proposed that aqueous dimethylsulfide (DMS) emissions, through a series of biological, physical and chemical processes, form the majority of CCN in remote, unpolluted marine air. These processes are is presented in Fig. 1. The rectangles are measurable quantities, while the ovals represent processes that may or may not be fully understood. First, waterborne DMS is excreted by various species of phytoplankton. This DMS, via an air-sea transport mechanism, is then ventilated to the atmosphere where it becomes oxidized. This upward flux, though not well defined, is dependent upon low-level wind speed and air/sea temperature differences. The result of this chemical reaction is the formation of two products: a methane sulfonate (MSA) and

a sulphate. The sulphate is thought to be the main product and is converted to non-sea-salt sulphate (NSS - SO_4^{2-}) particles.

These aerosols are abundant in the marine layer and are the principle CCN particles (Charlson et al. 1987). This is supported by the observation that sea-salt particle concentrations are usually not greater than 1 cm^{-3} and, on average, the observable CCN concentrations vary from 30 to 200 cm^{-3} (Pruppacher and Klett 1978). Therefore, sea-salt particles cannot be the main CCN source. At this point in the loop, there are two possibilities. The NSS - SO_4^{2-} particles may add mass to the existing CCN, which would tend to increase droplet radii. On the other hand, these particles could create new, and hence smaller, CCN. This change in size distribution would then affect the reflectance characteristics of the cloud. Holding the liquid water content (LWC) of the cloud constant, the number-density of droplets (N) and the droplet radius (r) are related by equation (1):

$$LWC = (4/3)\pi r^3 \rho N, \quad (1)$$

where ρ is the density (Charlson et al., 1987). Assuming that the NSS - SO_4^{2-} particles form new CCN, this would increase N and therefore decrease r . Twomey (1977) showed this decrease in droplet radius leads to an increase in total surface area and hence an increase in cloud albedo. Whereas the nuclei caused only minimal interaction with solar radiation because of their small size, the resultant change in cloud droplet density/size has a significant impact, as discussed by Coakley et al. (1987).

Continuing around the loop, the measurable increase in cloud albedo will decrease the surface temperature of the earth due to less incoming solar irradiance. However, the surface temperature is one of the factors pertinent to marine phytoplankton growth. It is not known whether less solar radiation would have a positive or negative effect on the production of DMS by marine phytoplankton. This production provides either positive or negative feedback to the aqueous DMS emissions, the initial step of Charlson's process.

A. RADIATIVE PROCESSES

To better understand the radiative processes which will be used to measure the expected change in cloud albedo, the following theoretical background is presented. Incoming solar radiation, upon reaching the earth's atmosphere, may be transmitted or attenuated. This attenuation, which includes absorption and scattering, is dependent upon such factors as atmospheric composition and electromagnetic wavelength. The

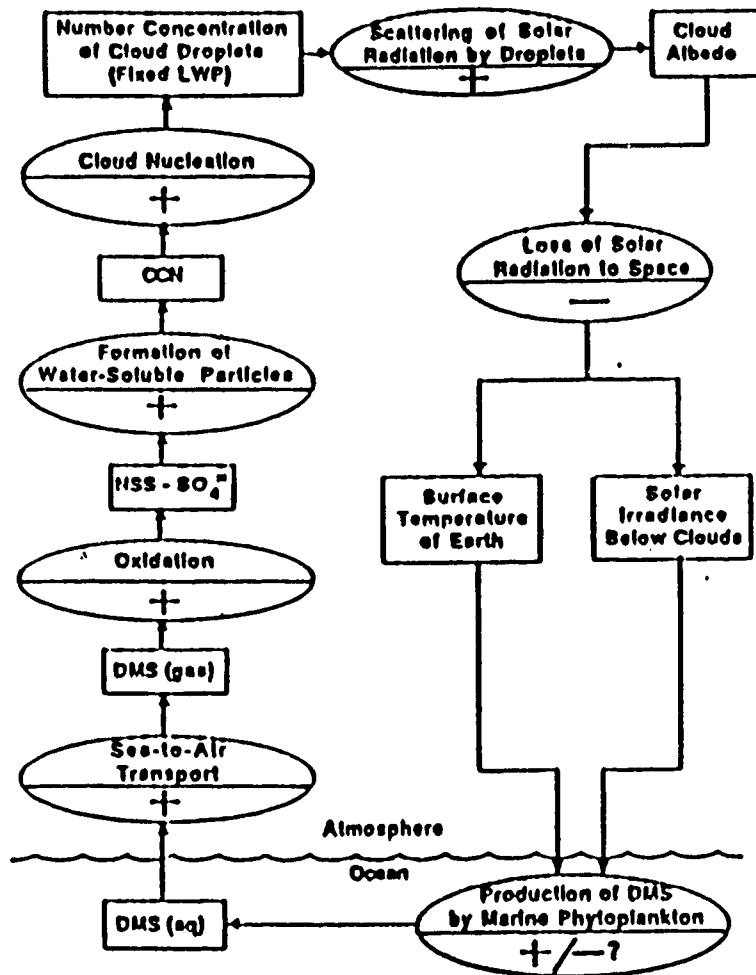


Figure 1. Conceptual diagram of a possible climatic feedback loop. The rectangles are measurable quantities and the ovals are processes linking the rectangles (Nature, 326, p. 659, 1987).

Fig. 1. Conceptual Diagram of Possible Climate Feedback Loop.: The rectangles are measurable quantities and the ovals are processes linking the rectangles, from Charlson et al. (1987).

AVHRR sensor onboard NOAA-7 measures $.63 \mu\text{m}$, $3.7 \mu\text{m}$ and $11.0 \mu\text{m}$ wavelengths for channels 1, 3 and 4, respectively. These wavelengths are located in atmospheric absorption "windows," where the incoming electromagnetic energy is mainly affected by scattering.

When the particle radius is approximately equal to the incoming energy wavelength, the dominant scattering process is defined by Mie theory (Liou 1980). Since DMS-produced non-sea-salt sulfate aerosols nucleate cloud droplet radii on the order of $10 \mu\text{m}$, Mie scattering dominates. Incident radiation in Mie processes tends to scatter in the forward direction relative to the incoming ray, rather than in the backward direction. Hunt (1972) presents phase diagrams for varying size distributions of cloud droplets, which emphasize that a decrease in particle size results in more backscattered radiant energy.

To evaluate the changes in cloud reflectance properties based on CCN/aerosol variations, it is necessary to examine both the channel 1 and channel 3 irradiance. Fig. 2 illustrates incoming solar radiation at channel 1 wavelengths ($.63 \mu\text{m}$) and channel 3 wavelengths ($3.7 \mu\text{m}$). First, channel 1 wavelengths are examined. Since there is no absorption at this wavelength, incoming photons are either transmitted through the cloud or scattered by cloud droplets. If the cloud thickness, Δz , is increased, there is less likelihood that energy will be transmitted through the cloud, thus increasing backscattered radiation. If the liquid water content (LWC) is increased, backscattered energy will also increase due to more interactions. Therefore, channel 1 reflectance is a function of size distribution, LWC and cloud thickness and it is difficult to predict variations in reflectance values at this wavelength without making limiting assumptions.

For channel 3 reflectance, on the other hand, the dependence on LWC and cloud thickness is not nearly as great as the dependence on droplet radius. Coakley and Davies (1986) suggest the sensitivity of reflectance to droplet radius in channel 3 is greatest due to moderate absorption at $3.7 \mu\text{m}$. Therefore, there is virtually no transmission through the cloud at this wavelength. This suggests cloud thickness and LWC variations do not appreciably affect the cloud reflectance. The reflectance at channel 3 wavelengths would increase based on injection of smaller CCN which leads to smaller and more numerous cloud droplets.

This point is further illustrated by Mineart (1988) who compared strato-cumulus cloud reflectance to mean droplet radius at both channel 1 and channel 3 wavelengths. Fig. 3 shows this comparison for stratocumulus measurements off the coast of southern California. There is no direct correlation of channel 1 with droplet size due to the

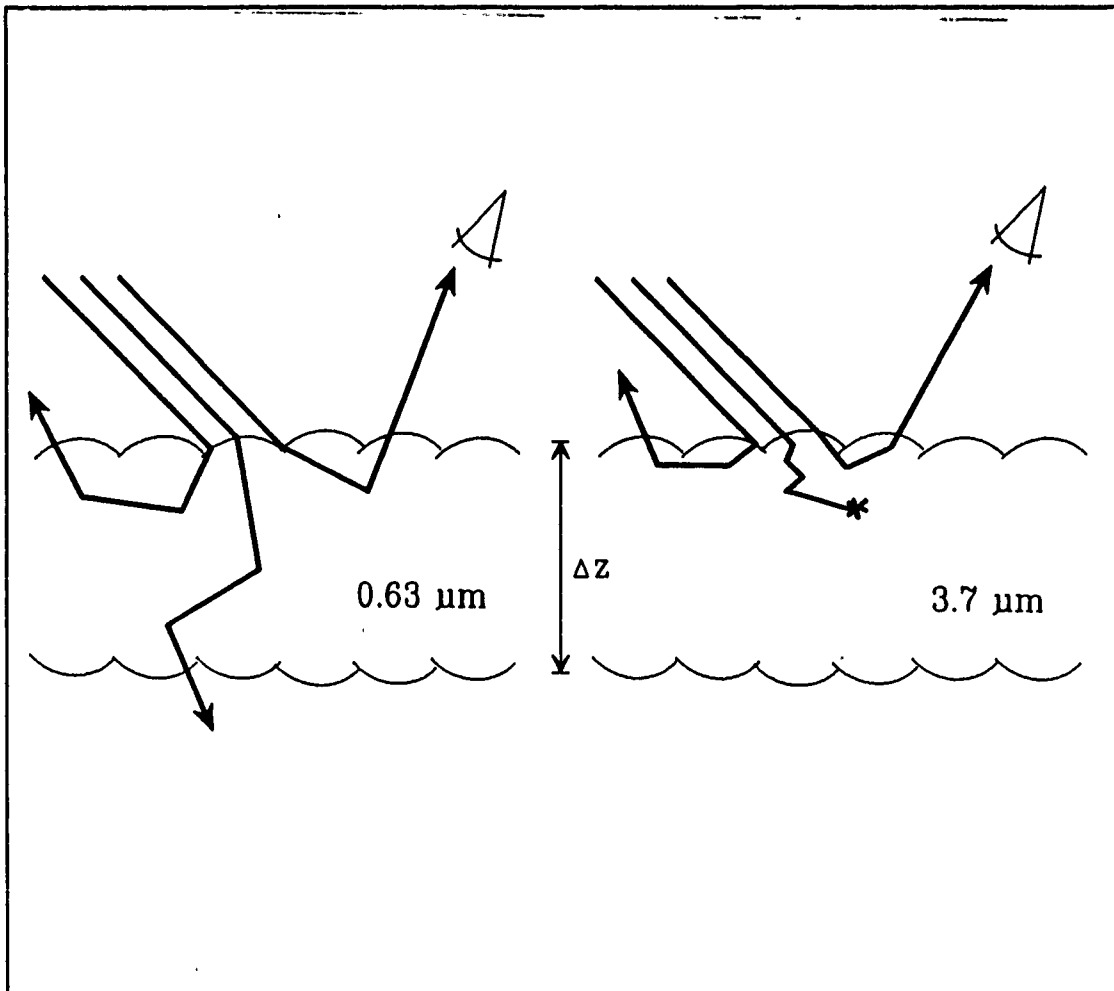


Fig. 2. Schematic of visible ($0.63 \mu\text{m}$) and near-IR ($3.7 \mu\text{m}$) energy interactions with clouds.

competing effects of size distribution with cloud thickness and LWC. However, for channel 3 there is a strong linear correlation such that as mean droplet radius increases, channel 3 reflectance decreases. This suggests that changes in cloud reflectance based on size distribution is more observable using channel 3 information.

B. MOTIVATION

This study will focus on the reflectance characteristics of clouds in the vicinity of DMS sources. The motivation for this project stems from silicon anomaly information obtained from the Marine Research Institute, Iceland, in the Denmark Strait near Iceland shown in Fig. 4. The species *Phaeocystes pouchetti* was dominant in the

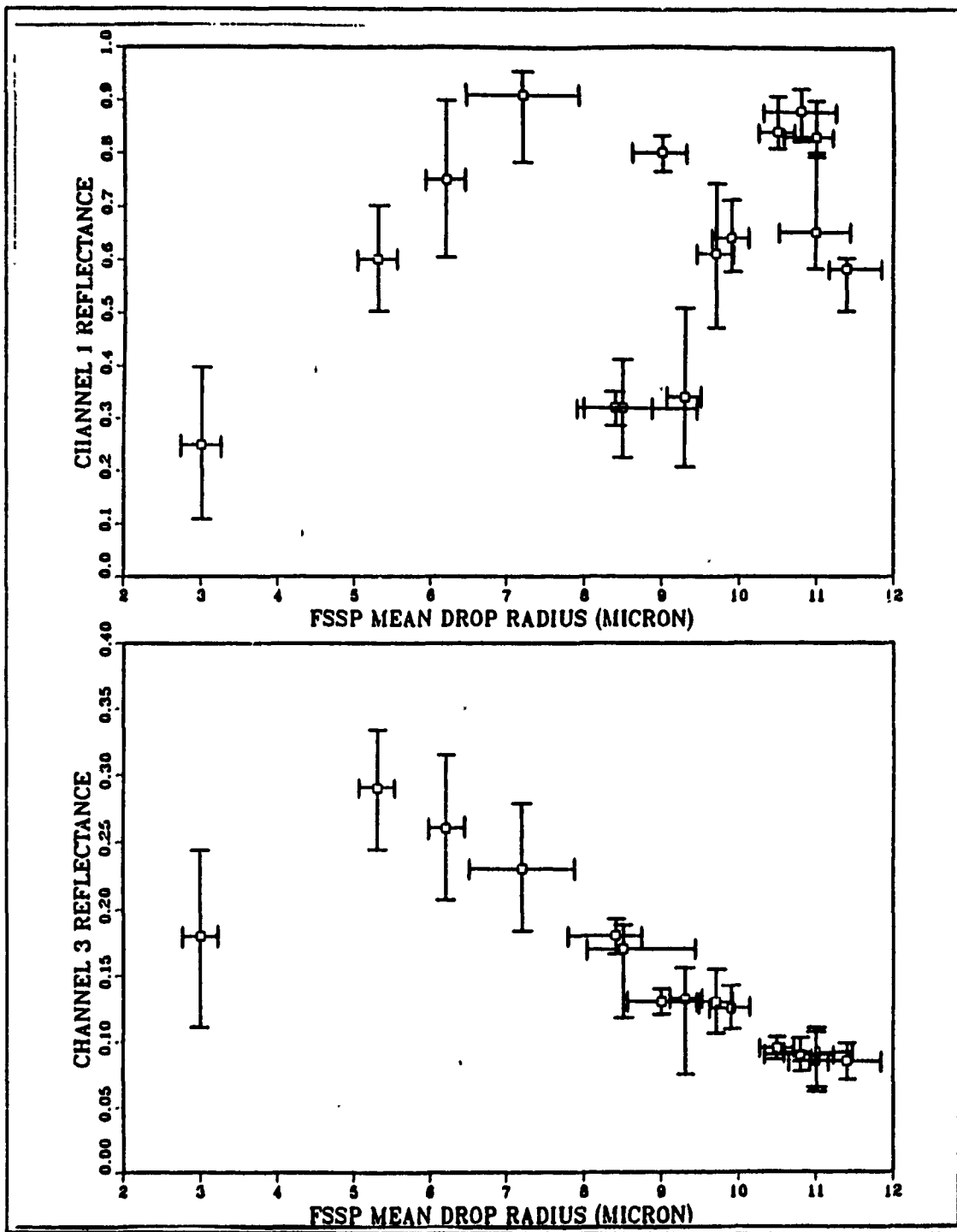


Fig. 3. Channel 1 ($.63 \mu\text{m}$) and channel 3 ($3.7 \mu\text{m}$) reflectance versus mean droplet radius, from Mineart (1988).

phytoplankton population in the Denmark Strait in the summer of 1984. *Phaeocystes pouchetti* is a known producer of DMS. This "bloom" of phytoplankton overwhelmed the existing diatom species which use silicon for growth and development, creating a measurable excess of silicon north of Iceland as depicted in Fig. 5. These silicon anomalies were measured between 24 May 1984 and 15 June 1984. The highest concentrations of silicon ($4 \mu\text{mol/L}$ greater than average) appear in the north and northwest portions off the Iceland coast. This can be compared to a "non-bloom" year such as 1982 as shown in Fig. 6. The only silicon anomaly is a small region north of Iceland where the values are $1 \mu\text{mol/L}$ greater than the average. The silicon anomaly information is used as an indirect measure of excess DMS.

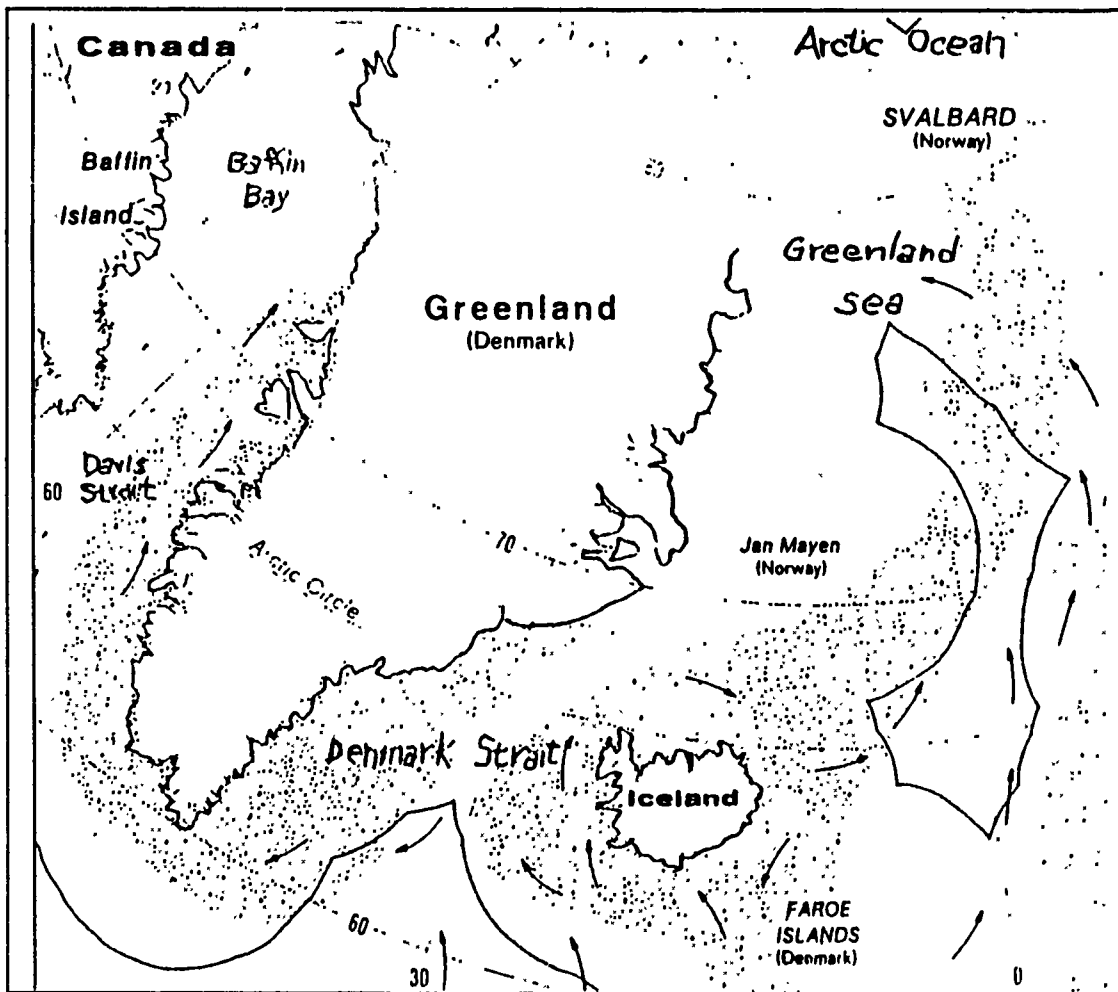


Fig. 4. Map showing Denmark Strait and the study analysis region.

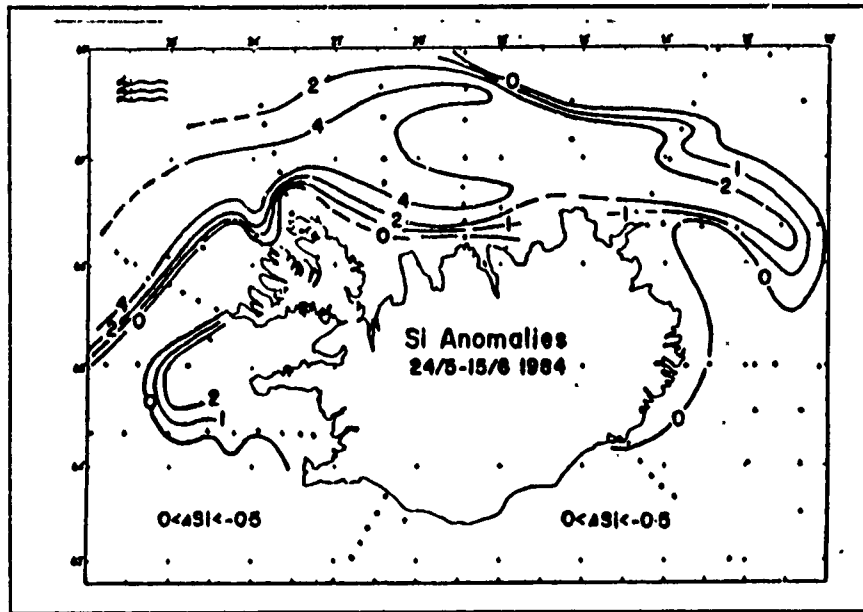


Fig. 5. Silicate anomalies ($\mu\text{mol/L}$) in the Spring of 1984 near Iceland, from Olafsson, 1988 (personal communication).

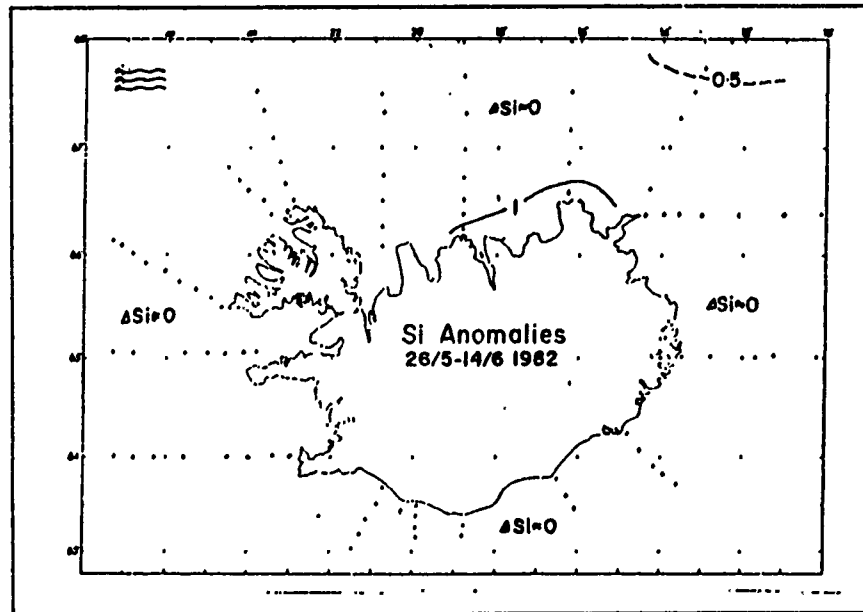


Fig. 6. Silicate anomalies ($\mu\text{mol/L}$) in the Spring of 1982 near Iceland, from Olafsson, 1988 (personal communication).

Motivation for study of these processes includes a climatic and an environmental perspective. Since the radiative processes of clouds play a major role in climate regulation, cloud reflectance information affecting the earth's heat budget is vital. In addition, the environmental cloud analysis aspect of this research is becoming increasingly important. Advanced weapon systems require accurate environmental inputs. With the advent of over-the-horizon weapons, it becomes even more critical to understand the variability of electro-optical properties of the atmosphere over a large area. Stratus clouds and low-level suspended particles affect weapon performance, especially those with low-level trajectories and/or terrain-following flight paths. Satellite reconnaissance efforts are also hampered in areas of persistent, stratus/stratocumulus clouds. Therefore, satellite measurements of these variations in cloud physics are vital.

C. OBJECTIVES

The purpose of this study is to examine aqueous dimethylsulfide (DMS) sources and their subsequent effects on cloud reflectance characteristics. This will be accomplished using NOAA-7 Advanced Very High Resolution Radiometer (AVHRR) satellite data in the visible, near-infrared and infrared portions of the electromagnetic spectrum. In order to determine whether DMS sources have any effect on reflectance properties of clouds, two cases will be compared. June 1982 ("non"-DMS-"bloom") data will be contrasted with June 1984 (DMS-"bloom") data in the vicinity of the Denmark Strait. Both individual AVHRR passes as well as composite images for the two years will be examined. Speculative results will be presented in regions where DMS source information is unavailable.

II. DATA ANALYSIS

A. DATA ACQUISITION/DESCRIPTION

The data sets used in this thesis were obtained from the AVHRR sensor onboard the NOAA-7 satellite. This satellite is from the TIROS-N family and is in a near-polar, sun-synchronous orbit with a nominal altitude of 833 km. Maximum resolution of data at satellite sub-point is 1.1 km x 1.1 km. Global Area Coverage (GAC) data for nine days in June 1982 and seven days in June 1984 were examined. The use of GAC data, which minimizes archiving requirements, reduces the resolution to approximately 4.0 km X 4.0 km. This is due to the fact that GAC data contains only one out of three original AVHRR lines as well as averages every four of five scan positions (Kidwell 1986). The area of interest for this study is bounded by 60° and 70° north latitude and 0° and 30° west longitude. The focus of the analysis is the area of silicon anomalies in the Denmark Strait between Iceland and Greenland.

B. DATA PROCESSING

Processing was performed in the Interactive Digital Environmental Analysis (IDEA) Laboratory located at the Naval Postgraduate School in Monterey, California. Processing began by gleaning the data from archived magnetic tapes obtained from the National Oceanic and Atmospheric Administration (NOAA). Due to the severe distortion in the horizontal at the edges of the AVHRR passes, a remapping of all images was performed into an orthographic projection. The scale of this projection is true at the center and decreases radially with distance from the center. Since the area of concern is nearly centered in the projection, little distortion is expected. Once remapped, channel 1, channel 3 and channel 4 images were produced from each pass. The radiance values for each channel were calculated using the equation

$$L = \epsilon B(T) + r(\theta_0, \theta, \phi) I \cos \theta, \quad (2)$$

where L is the satellite-measured radiance, ϵ is the emissivity, $B(T)$ is the blackbody intensity, r is the reflectance of the medium and I is the incident solar radiation. The reflectance is a function of solar zenith angle (θ_0), satellite zenith angle (θ) and relative azimuth (ϕ). The first term of equation (2) is the thermal emittance (dominant in IR wavelengths), whereas the second term is the backscattered solar radiation (dominant in

visible wavelengths). The sum of these two approximate the total radiance from the source. A brief description of each channel follows.

1. Channel 1.

Channel 1 (.58-.68 μm) is strictly backscattered solar radiance. Therefore, the first right hand term in equation (2) is zero. Channel 1 is calibrated in terms of albedo and is a measure of bi-directional reflectances (Lauritson et al. 1979). This radiance is further corrected using the anisotropic reflectance factor (ARF). The ARF is a method of reducing the sun-satellite geometry dependence of reflectance so that all images, regardless of solar zenith angle (SZA), can be accurately compared. Taylor and Stowe (1984) developed an atlas of ARF's using empirical methods to apply geometric corrections based on surface type, SZA, satellite zenith angle and relative azimuth. A total of eight surface types (land, water, snow, ice, low/middle/high water clouds and high ice clouds) were examined. Since low clouds are the focus of this study, channel 1 images were corrected using low cloud anisotropy and this will be referred to as a "LOW1" image. An example of a "LOW1" image is given in Fig. 7. The pixel values represented in grayshades from 0-255 correspond to reflectance values from 0-100%.

2. Channel 3

Channel 3 (3.55-3.93 μm) includes not only backscattered solar radiance (as in channel 1), but also includes thermally emitted radiance. Therefore, both terms of equation (2) contribute to channel 3 radiances. The undesirable thermal radiance was removed using a technique devised by Allen (1987). It uses channel 4 brightness temperature to separate the two emittances. As with channel 1, the ARF correction is implemented to produce a "LOW3" image. An example of a "LOW3" image is given in Fig. 8. Pixel values represented in grayshades from 0-255 correspond to reflectance values from 0-40%. Instrument noise can cause some interference in channel 3 signals, but this interference is minimal for the cases presented here because the images were produced from daytime passes, when higher energy levels are present relative to the interference.

3. Channel 4

Channel 4 (10.3-11.3 μm) is a brightness temperature derived from thermal emittance from both surface and atmospheric elements. The second right hand term in equation (2) is therefore eliminated. Processes involved in converting this emittance to a temperature include utilization of the Planck function and temperature corrections from the NOAA calibration manual (Lauritson et al. 1979). Brightness temperatures between 320 K and 256 K were displayed using grayshades from 0-255. Hence a pixel



Fig. 7. LOW1 (AVHRR channel 1, low-cloud anisotropy corrected) image at 1415 UTC on 12 June 1982.

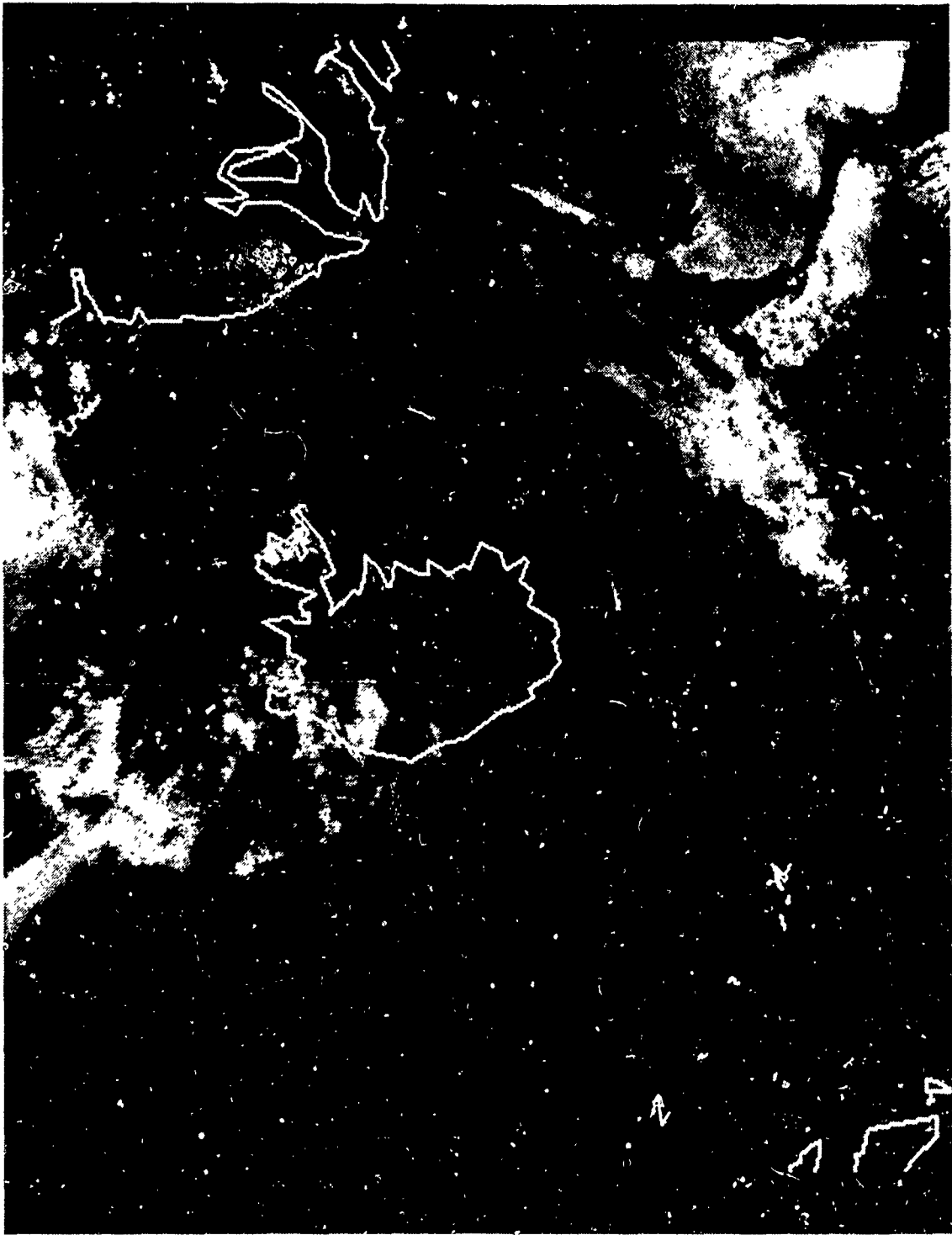


Fig. 8. LOW3 (AVHRR channel 3, low-cloud anisotropy corrected) image at 1415 UTC on 12 June 1982.

value of 64 corresponds to a brightness temperature of 304 K and a pixel value of 192 corresponds to a temperature of 272K. The channel 4 images will be referred to as "TEMP4" images for the remainder of this study.

4. Composite Images

After processing a LOW1, LOW3 and TEMP4 image for each of the satellite passes in the data sets, composite images of June 1982 and June 1984 were created. This was accomplished using an averaging algorithm on each 512 X 512 pixel image for a particular day. Fig. 9 illustrates this process. First, the three images were subject to two criteria, pixel by pixel. The first test checks the LOW1 values. If the value is less than 20% reflectance, it is assumed to be a cloud-free pixel, and the data are not used. A threshold of 20% is an accepted boundary between cloud and cloud-free regions. The second test involves the TEMP4 value. Since the focus of this study is on low clouds, a TEMP4 cutoff of 267.5K was instituted. Any pixel value greater than this temperature was assumed to be high cloud. These data also were not used due to contamination of low cloud information. Once each set of three images was tested for the nine days in June 1982 and the seven days in June 1984, those pixels successfully meeting the two criteria were averaged, producing a LOW1 composite and a LOW3 composite for each year. For ease of quantitative comparison, all LOW1, LOW3, TEMP4 and composite images used in this study were color enhanced.

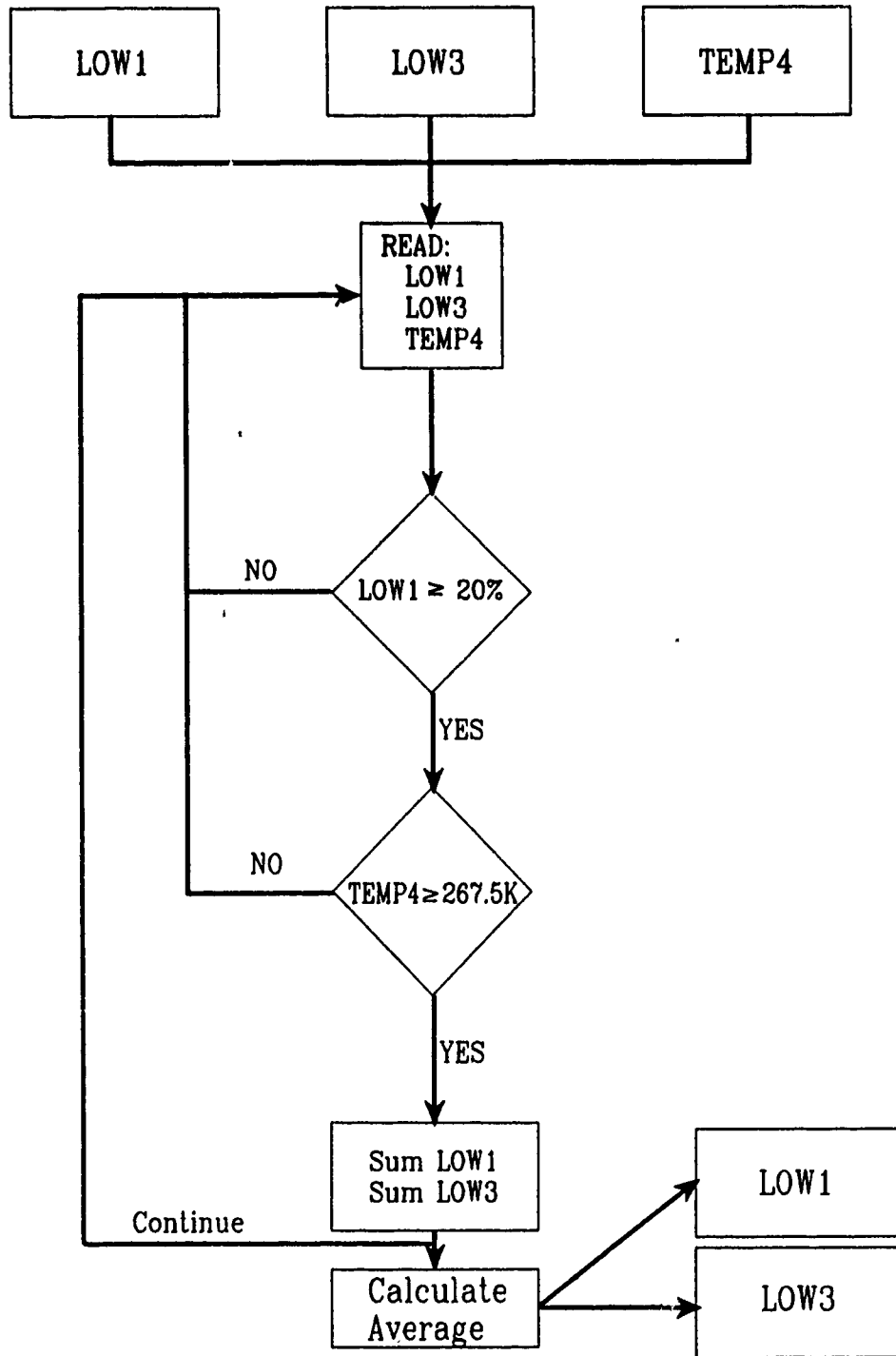


Fig. 9. Flowchart illustrating composite averaging algorithm.

III. RESULTS

This section will discuss the results obtained from the June 1982 and June 1984 data sets. First, representative days from each of the two years will be discussed, focusing on individual features of each pass. Case 1 consisted of two AVHRR passes, one on 12 June 1982 and another on 13 June 1982. Case 2 also consists of two passes, one on 9 June 1984 and one on 13 June 1984. Second, composite images from 1982 and 1984 will be examined, concentrating on comparisons of radiance values from channel 1 and channel 3. Finally, the composite images will be divided into sectors based on surface wind analyses and silicon anomaly information, which infers excess DMS. Specific conclusions will be drawn in areas where silicon anomalies exist. Regions where no inferred-DMS source information exists are also analyzed.

A. CASE 1. SAMPLE 1982 DATA SET

1. Synoptic Overview for June 1982

The 1200 UTC surface analysis on 12 June 1982 (Fig. 10) is representative of the surface situation throughout the June 1982 period. A high pressure center of 1031 mb is located 500 n mi to the northwest of Iceland while a low pressure center of 992 mb is located 900 n mi to the southeast. The pressure gradient nearer the low is producing northeast winds of up to 25 kt to the extreme southeast of Iceland. However, near the Denmark Strait the pressure gradient is weaker and surface winds are from the north-northeast at 5-10 kt.

2. AVHRR Analysis for 12 June 1982 (Case 1A)

Figs. 11, 12 and 13 illustrate the LOW1, LOW3 and TEMP4 images at 1415 UTC on 12 June 1982. Fig. 11 reveals cloud-free areas to the north, southeast and south of Iceland adjacent to the coast. The area on the extreme southern edge of the image south of Iceland as well as a small circular area south of Greenland also are clear. The rest of the region is dominated by clouds, with the highest reflectance values located in a broad band directly west of Iceland (red/purple). Fig. 13 shows severe high cloud contamination to the west of Iceland (black) with moderate, patchy contamination near Greenland (dark purple/black). The LOW3 analysis will not include these areas as illustrated by Fig. 9 due to the focus of this study on low clouds.

Fig. 12, in general, shows scattered/broken stratus clouds. To the north of Iceland at point "A", LOW3 reflectance values are 7-10% (light blue). To the south at

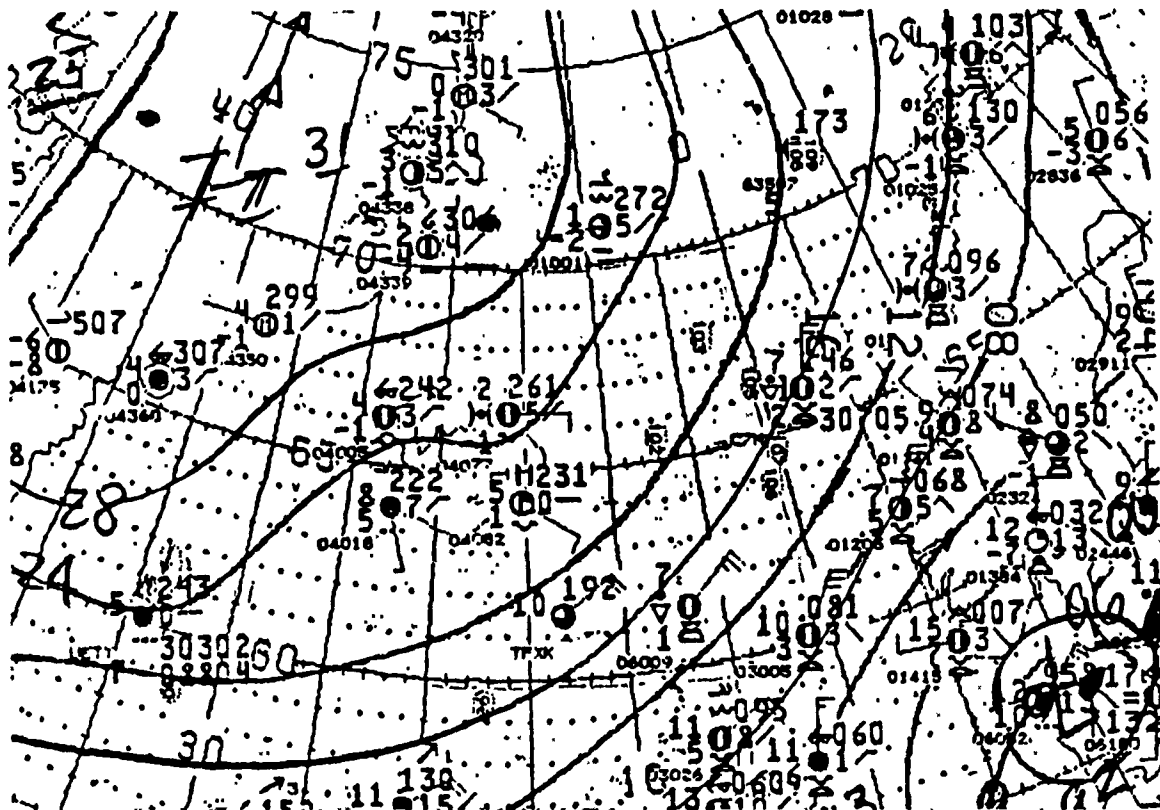


Fig. 10. Mean sea-level pressure analysis and plotted surface data for 1200 UTC on 12 June 1982.

point "B", the main stratus area shows values between 8-12% (light blue). At point "C" located to the southwest, the stratus deck indicates radiance values ranging from 9-22% (light blue to yellow). Reflectance values up to 24% (yellow) are also found in two narrow bands located to the far northeast of Iceland at points "D" and "E". However, the vast majority of reflectance values in this image are between 7-12% (light blue).

3. AVHRR Analysis for 13 June 1982 (Case 1B)

The purpose of this subscene is to provide coverage in the high cloud contamination regions in Case 1A. Figs. 14, 15 and 16 display the three channels of this 1403 UTC pass for 13 June 1982. Figure 14 indicates that a band of low clouds are present to the west of Iceland and along the southern edge of Greenland. A check of Fig. 16 reveals that these particular areas are not contaminated by high clouds. The majority of the associated LOW3 radiances (Fig. 15) of the clouds to the northwest of Iceland range from 9-16%

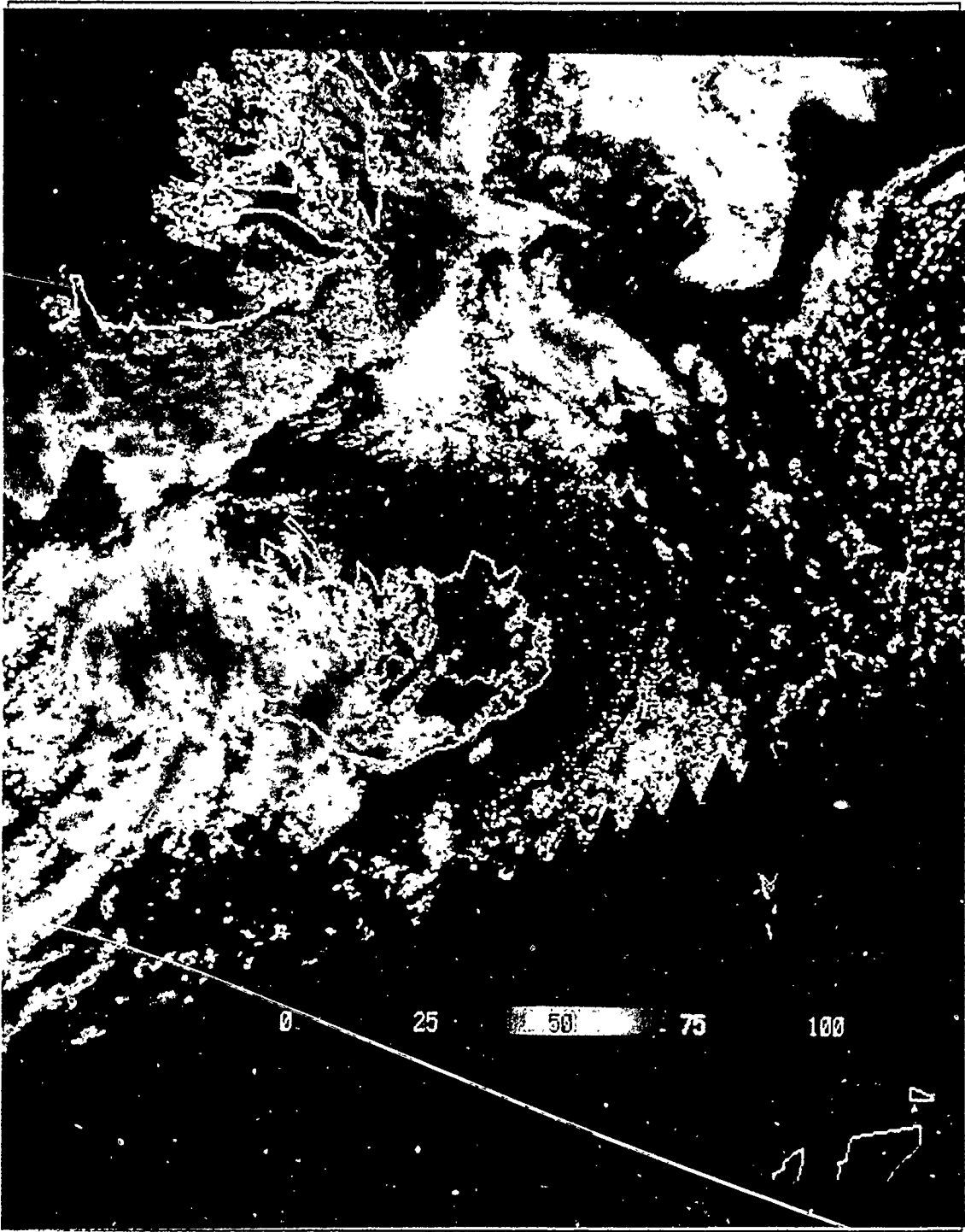


Fig. 11. LOW1 image for 1415 UTC on 12 June 1982.

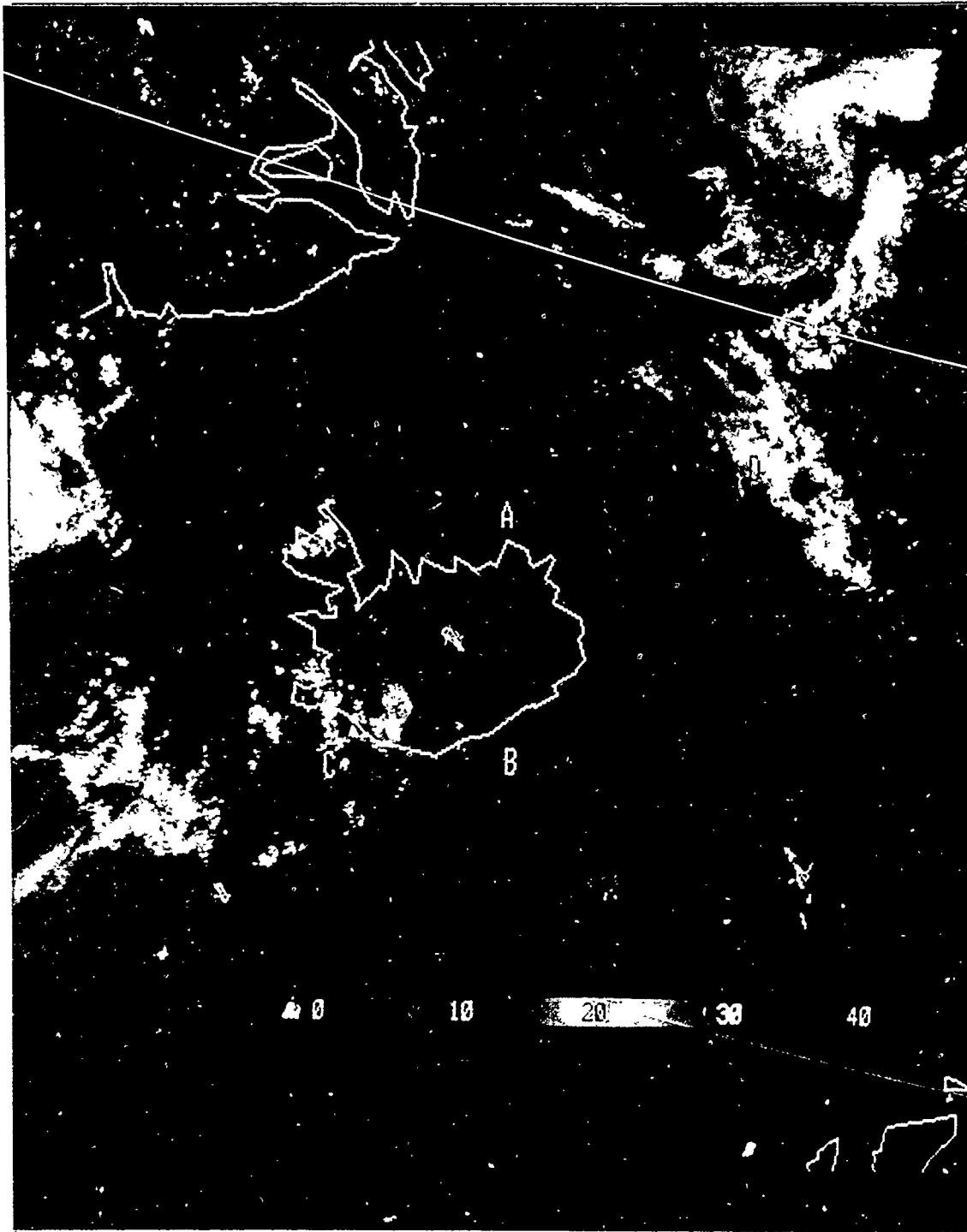


Fig. 12. LOW3 image for 1415 UTC on 12 June 1982.

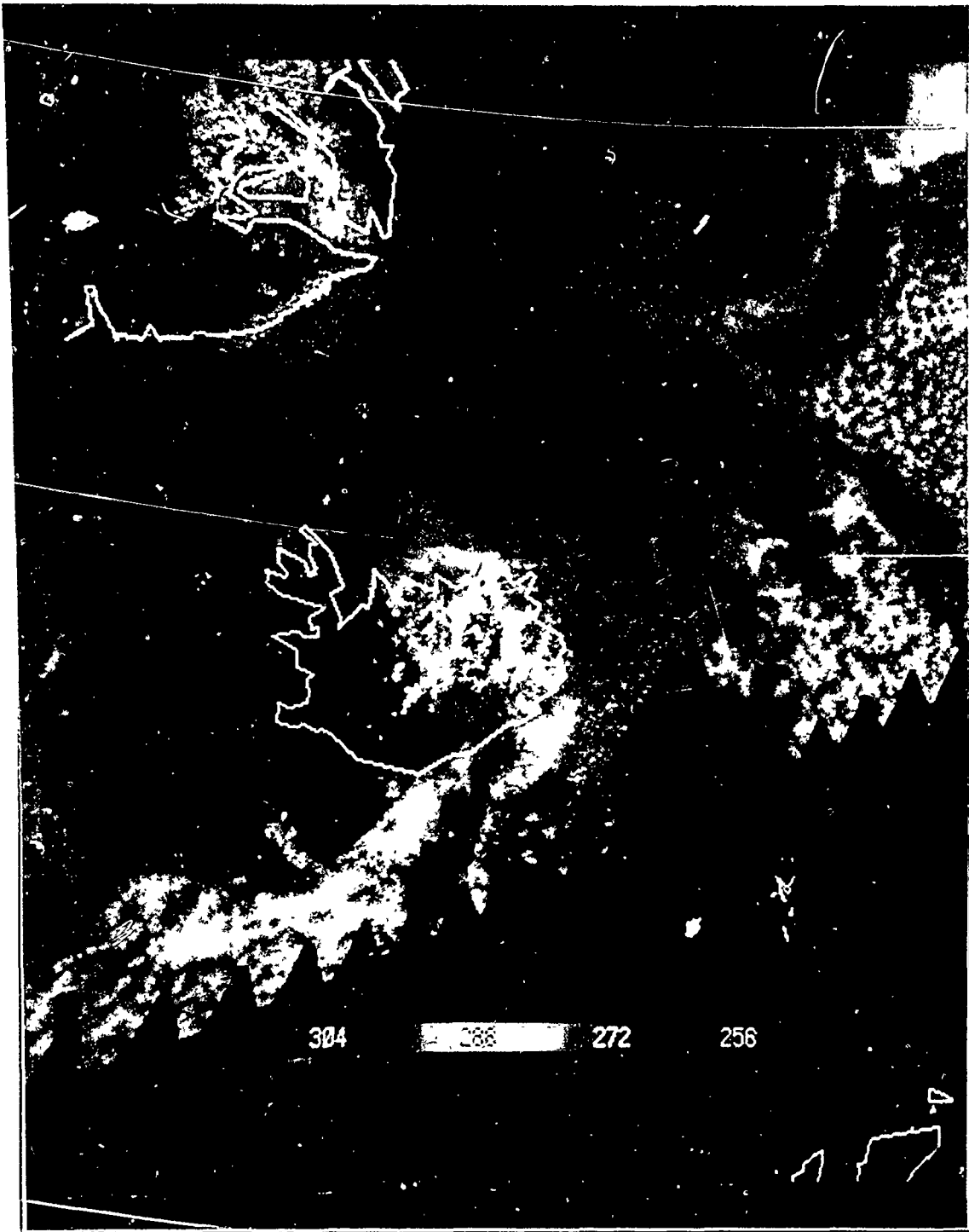


Fig. 13. TEMP4 image for 1415 UTC on 12 June 1982.

(light blue/green) with two extremely small areas where the reflectances reach as high as 24% (yellow) at points "F" and "G". Directly to the west of Iceland a well compacted cloud area below "F" with LOW3 values of 7-12% (light blue) is dominant. To ensure confidence of the 12 June 1982 findings, a check of LOW3 reflectance values to the north and east of Iceland was performed. These values were consistent with the 12 June 1982 results in that LOW3 reflectance values are generally between 10-15% (light blue/green).

B. CASE 2. SAMPLE 1984 DATA SET

1. Synoptic Overview for 1800 UTC on 13 June 1984

The 1800 UTC surface analysis (Fig. 17) for 13 June 1984 is representative of the surface situation for the June 1984 timeframe, the period of silicon anomalies. A 1018 mb high pressure center is located 600 n mi to the north-northwest of Iceland and a 1001 mb low pressure center is located 800 n mi to the east. The pressure gradient is weak over Iceland; hence the surface winds are from the northwest at 5-10 kt.

2. AVHRR Analysis for 9 June 1984 (Case 2A)

Figs. 18, 19 and 20 show the 0941 UTC AVHRR images for the three channels for 9 June 1984. Fig. 18 reveals the cloud-free areas are restricted mainly to small regions to the extreme north, northeast and east of Iceland (light blue). Otherwise, the area is covered by broken/scattered cloud coverage, with an overcast band to the south of Iceland (yellow/red). Examination of the TEMP4 image (Fig. 20) shows severe high cloud contamination west of Iceland (black), as well as moderate contamination to the southwest and to the far northeast (dark purple/black). This figure also displays distinct contrail patterns to the south of Iceland. Hence, as with Case 1A, conclusions about these regions of the subscene cannot be made.

LOW3 reflectance values (Fig. 19) to the north of Iceland vary widely, from 13-30%. The highest values in this area are near "H", a narrow east-west band (yellow/red). To the northeast of Iceland in the non-contaminated region, the LOW3 values range from 9 to 22% (light blue to yellow), with the highest values as point "I" (yellow). To the southeast, the main stratus reflectance is between 14- 18%, but a distinct band imbedded within the stratus at point "J" shows values up to 24% (yellow).

Another interesting feature of fig. 19 is the extremely high reflectance values in an expansive region near point "K" in the far southeast corner of the image. LOW3 values range from 28-32% (yellow/red), and the TEMP4 data shows no high cloud contamination in this area. The cause of this feature leads to the possibility of another

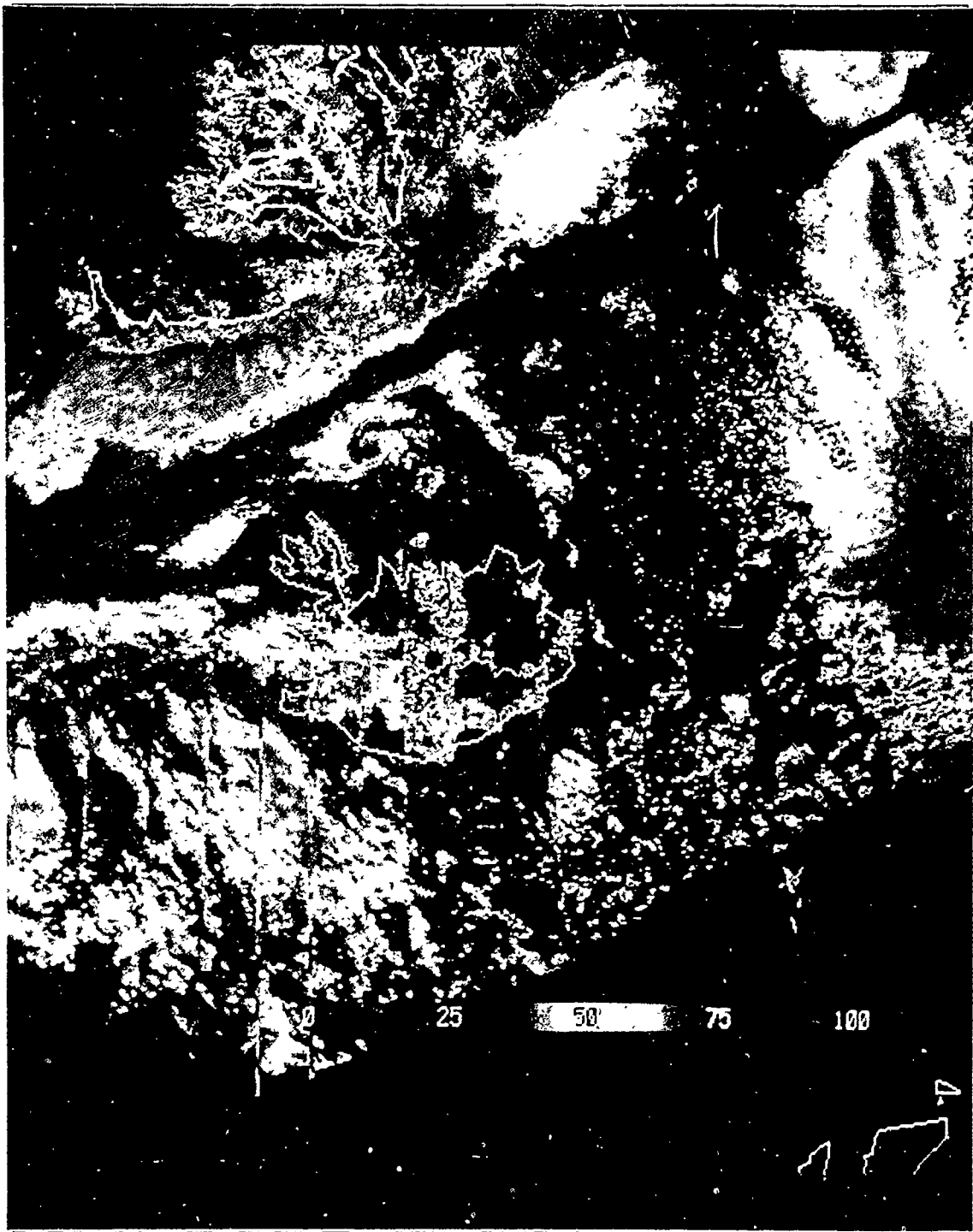


Fig. 14. LOW1 image at 1403 UTC on 13 June 1982.

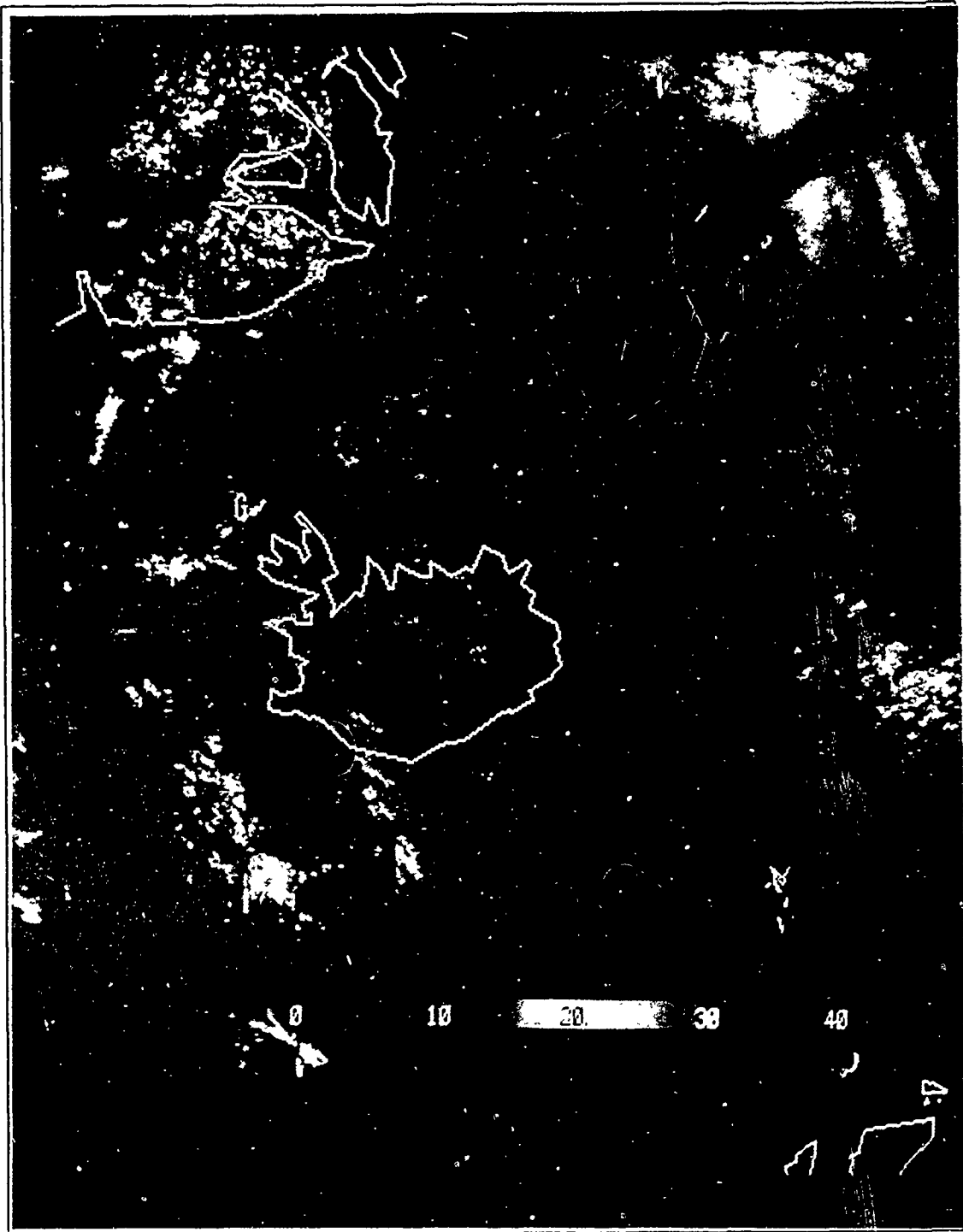


Fig. 15. LOW3 image at 1403 UTC on 13 June 1982.

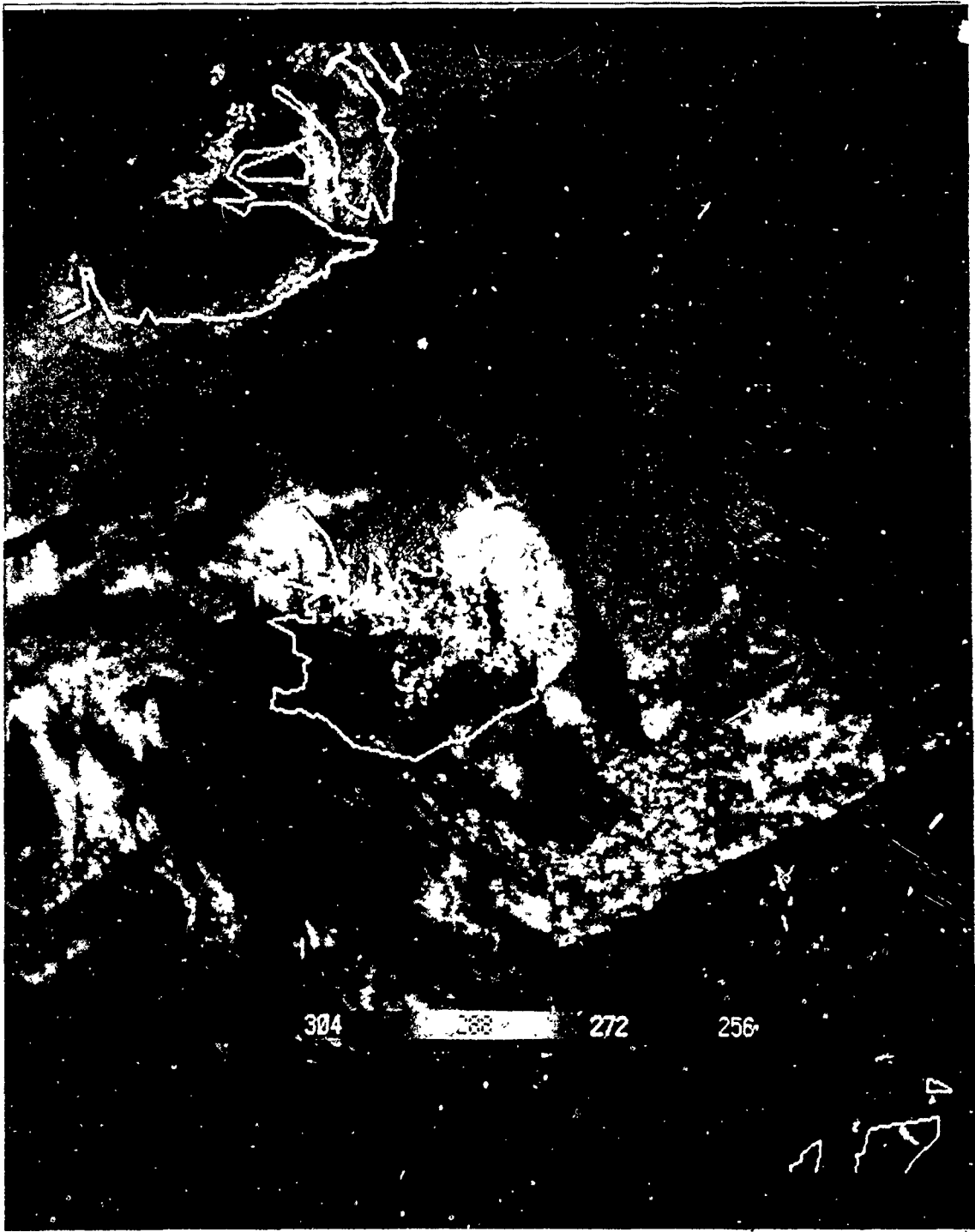


Fig. 16. TEMP4 image at 1403 UTC on 13 June 1982.

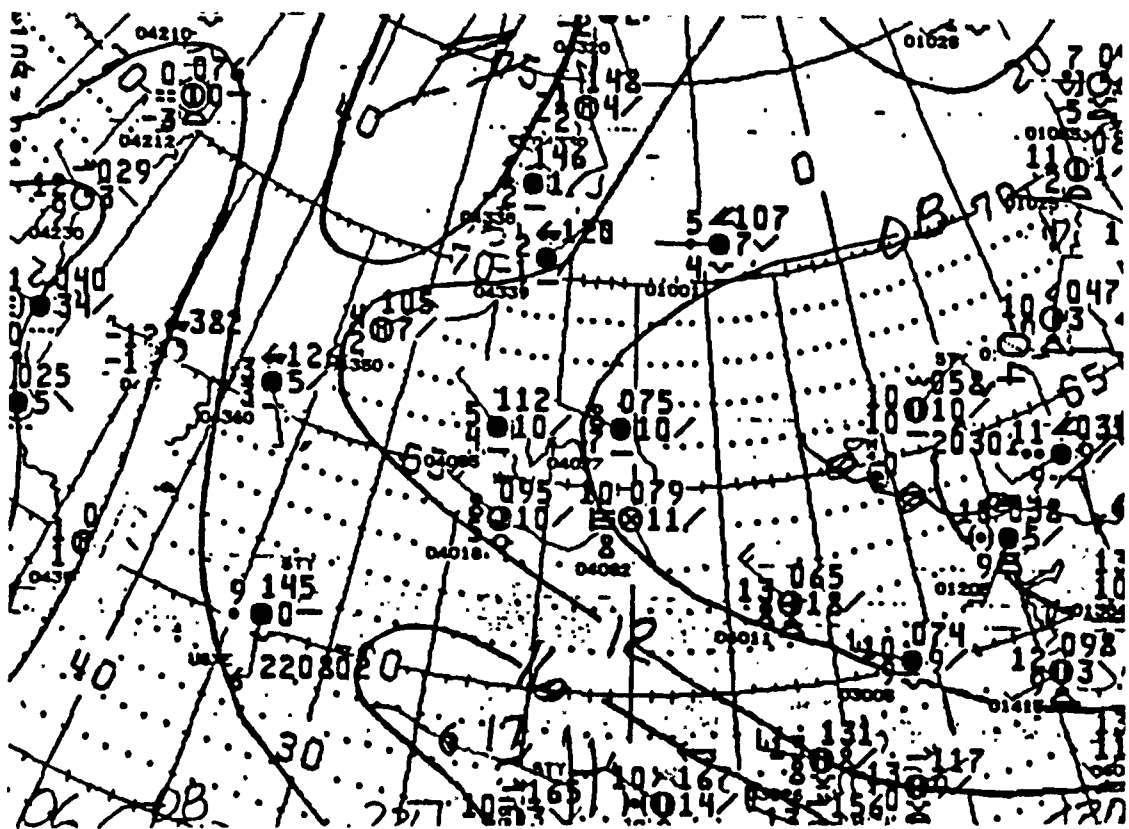


Fig. 17. Mean sea-level pressure analysis and plotted surface data for 0941 UTC on 13 June 1984.

bloom event of DMS-producers in this region. However, currently there is no silicon anomaly information for this area to substantiate this possibility.

3. AVHRR Analysis for 13 June 1984 (Case 2B)

Figs. 21, 22 and 23 show the three images for the 1655 UTC pass on 13 June 1984. As with the 1982 case, this subsene was chosen to eliminate the severe high cloud contamination observed in case 2A directly west of Iceland. Fig. 21 shows a small clear area adjacent to the west coast of Iceland (dark blue/light blue) as well as a broader clear area further west. Fig. 22 indicates the low3 reflectance values range from 14-19% (green/yellow), with a small circular band of clouds at point "L" with values as high as 27% (yellow/red). In addition, a coherent band of clouds with reflectance values up to 30% (red) are located at point "M" southwest of Iceland. A cursory check of LOW3 values to the south and east of Iceland concurs with the results found for the 9 June



Fig. 18. LOW1 image for 0941 UTC on 9 June 1984.

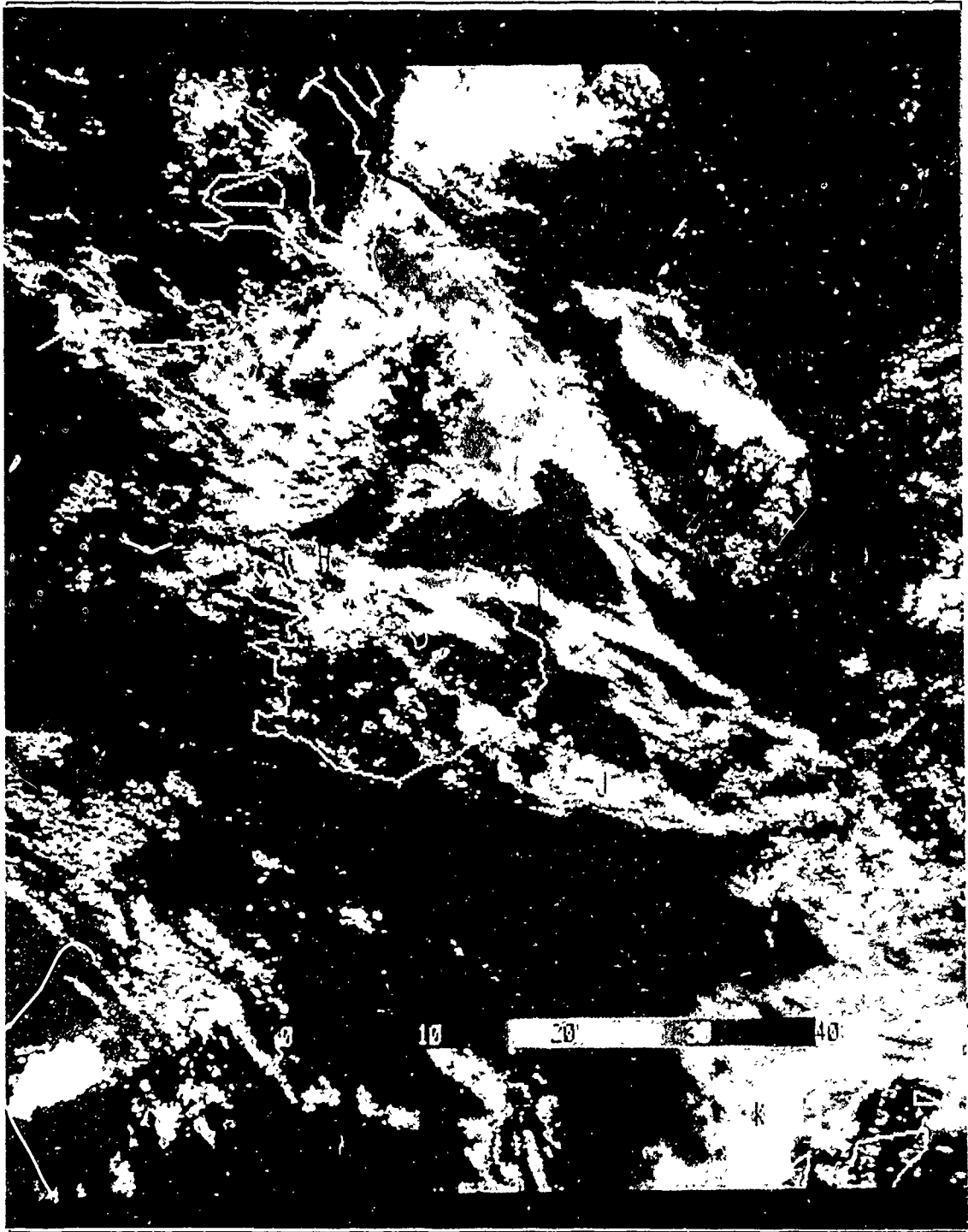


Fig. 19. LOW3 image for 0941 UTC on 9 June 1984.

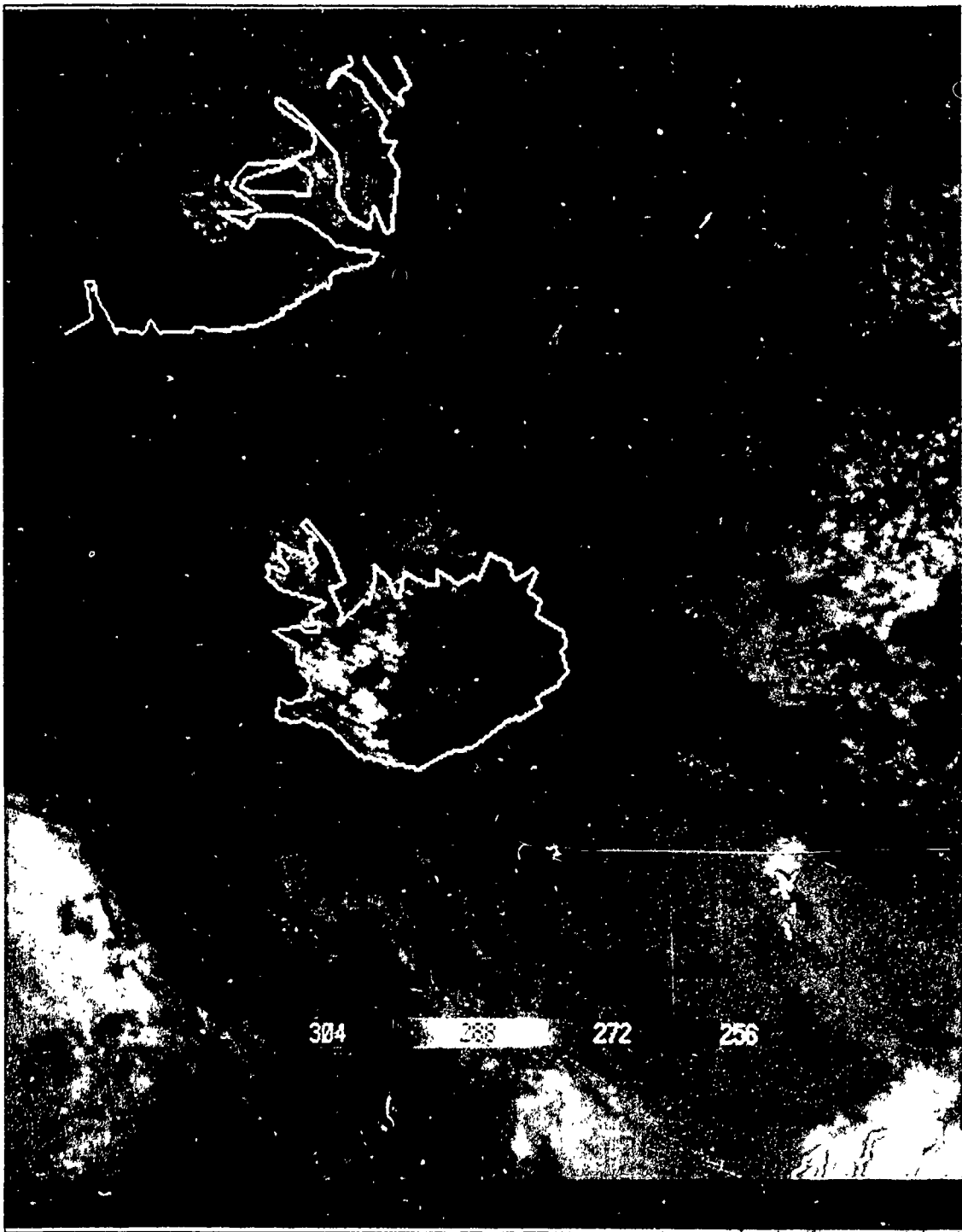


Fig. 20. TEMP4 image for 0941 UTC on 9 June 1984.

1984 case, such that the average LOW3 reflectance values near Iceland are 20-25%(yellow/red).

Although day-to-day differences exist within each of the individual day's images, comparisons can be made between the sample June 1982 data and the sample June 1984 data. Overall, the 9 June 1984 and the 13 June 1984 LOW3 images are on the order of 40% brighter than those of 12 June 1982 and 13 June 1982. The most notable increase in channel 3 reflectance in the June 1984 examples occurs to the north-northwest of Iceland. June 1984 sample data reveals representative LOW3 values of 20-25% (yellow/red) whereas June 1982 sample data shows values of 5-10% (light blue). This is consistent with the inferred-DMS source regions in June 1984 shown in Fig. 5.

C. COMPOSITE RESULTS

Figs. 24 and 25 shows the LOW1 composite results for June 1982 and June 1984. These composites for the nine days in 1982 and the seven days in 1984 should eliminate the day-to-day differences between individual images. Overall comparison of LOW1 reflectance values shows higher reflectance in the 1984 composite. Specifically, to the south of Iceland, the 1984 composite shows slightly higher reflectances (40-60% in June 1982 versus 60-75% in June 1984). To the east, 1984 shows significantly higher values, roughly 45-65% (yellow) as compared to 30-45% (light blue/yellow) in June 1982. To the north of Iceland, again the 1984 composite displayed reflectance values of approximately 30-50% (green/yellow), whereas the 1982 data shows values of 20-35% (light blue green). The only region in the vicinity of Iceland where the 1982 composite indicates higher reflectances is to the west/southwest. Here, both years show high LOW1 reflectances, but 1982 has values between 50-70% (yellow/red) whereas 1984 has values approximately 40-60% (green/yellow). Outside the Denmark Strait, the 1984 composite shows extremely higher reflectances in the southeast corner of the image. Reflectances in 1984 approach 75% (red) here. The majority of 1984 composite data in this area is based on a single AVHRR pass, and the 1982 composite shows a void of data in the extreme southeast corner. Nonetheless, the expanse of this high reflectance region warrants further investigation. In summary, the majority of LOW1 reflectance values are higher in the June 1984 composite compared to the June 1982 composite.

Figs. 26 and 27 show the LOW3 composite results for June 1982 and June 1984. The LOW3 values to the southwest of Iceland are higher in 1982. This "plume" of brightness (green/yellow) is suggestive of terrestrial sources since the prevailing winds during this timeframe were from the north-northeast. These values in 1982 range from

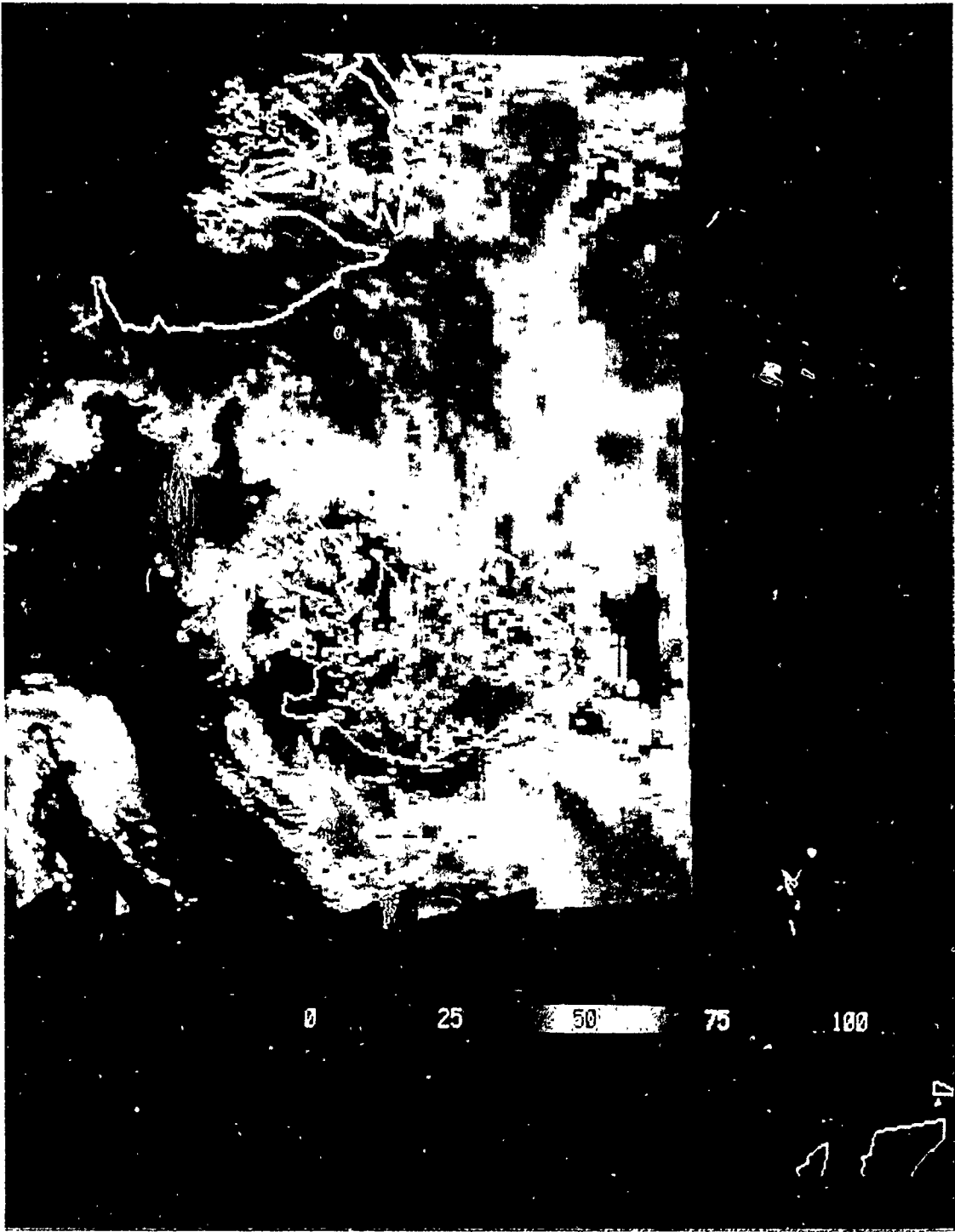


Fig. 21. LOW1 image for 1655 UTC on 13 June 1984.

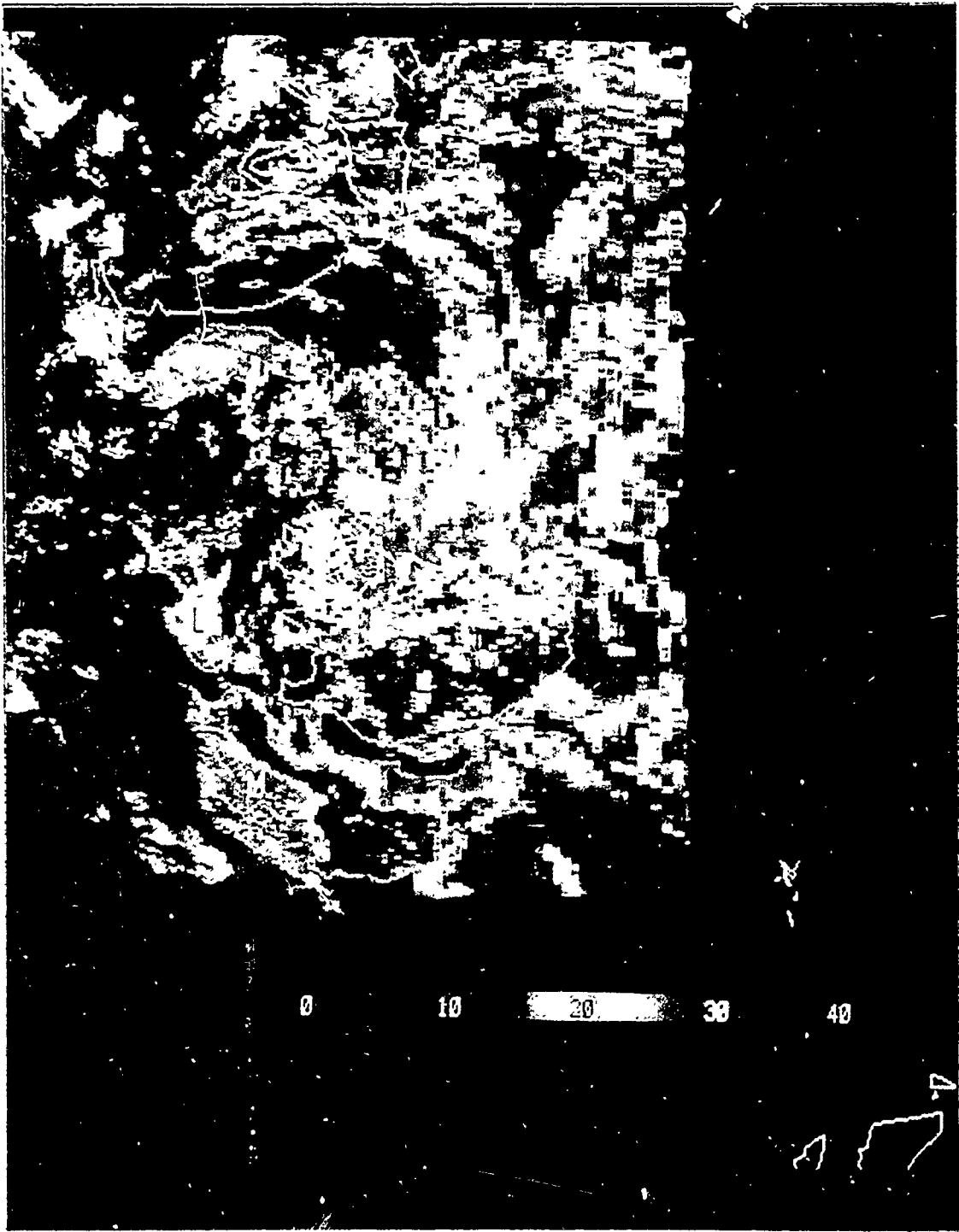


Fig. 22. LOW3 image for 1655 UTC on 13 June 1984.

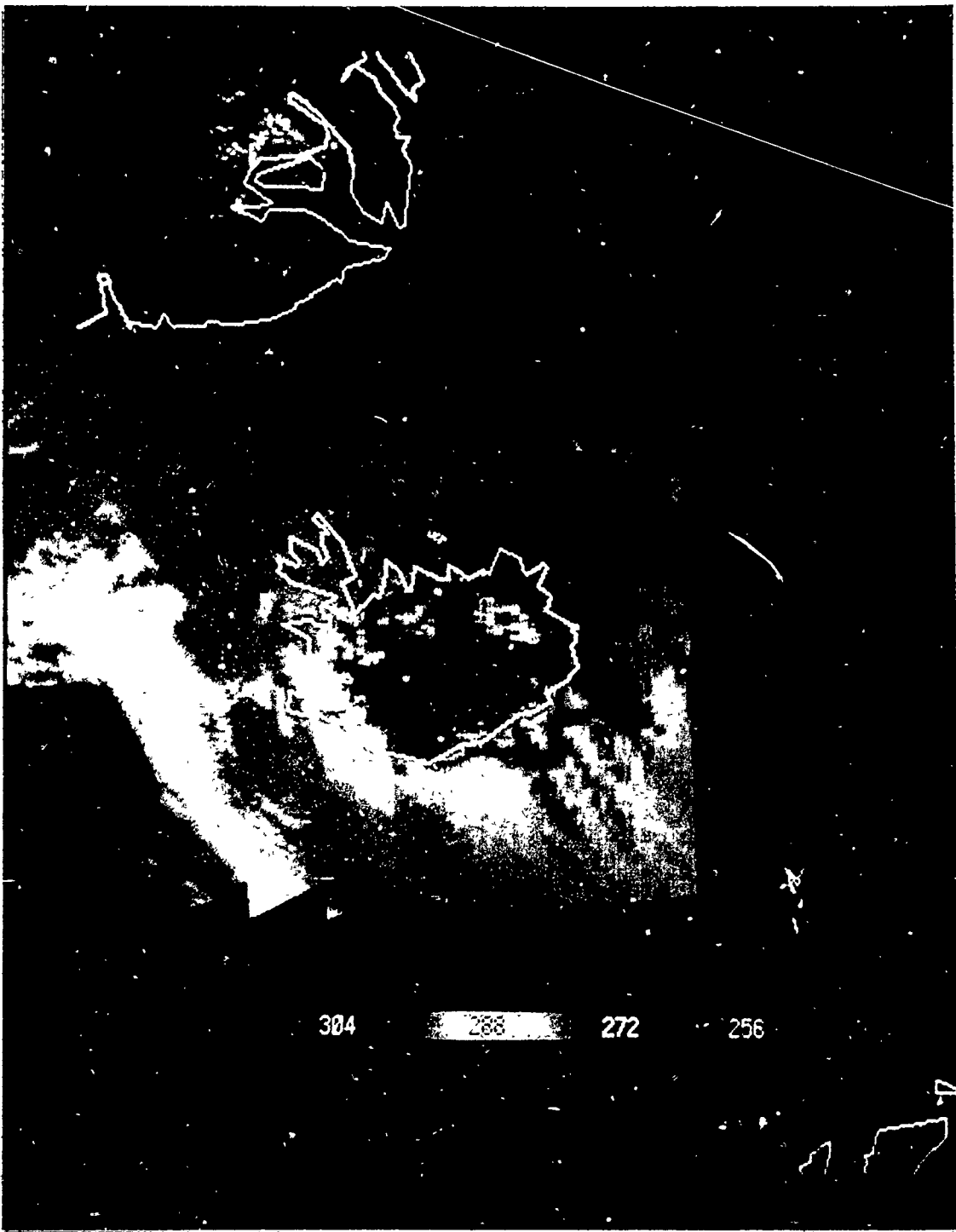


Fig. 23. TEMP4 image for 1655 UTC on 13 June 1984.



Fig. 24. LOWI composite for June 1982.



Fig. 25. LOW1 composite for June 1984.

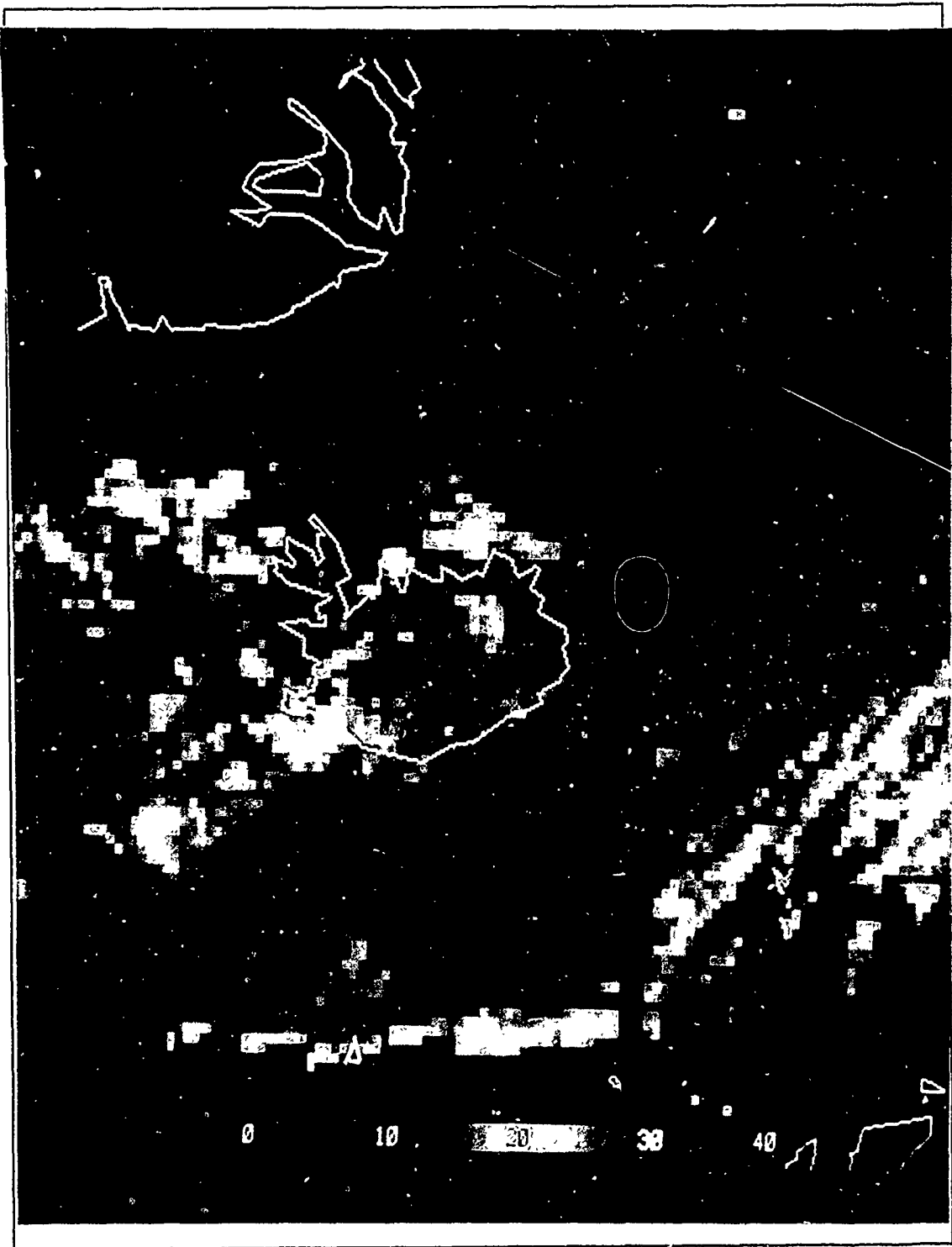


Fig. 26. LOW3 composite for June 1982.

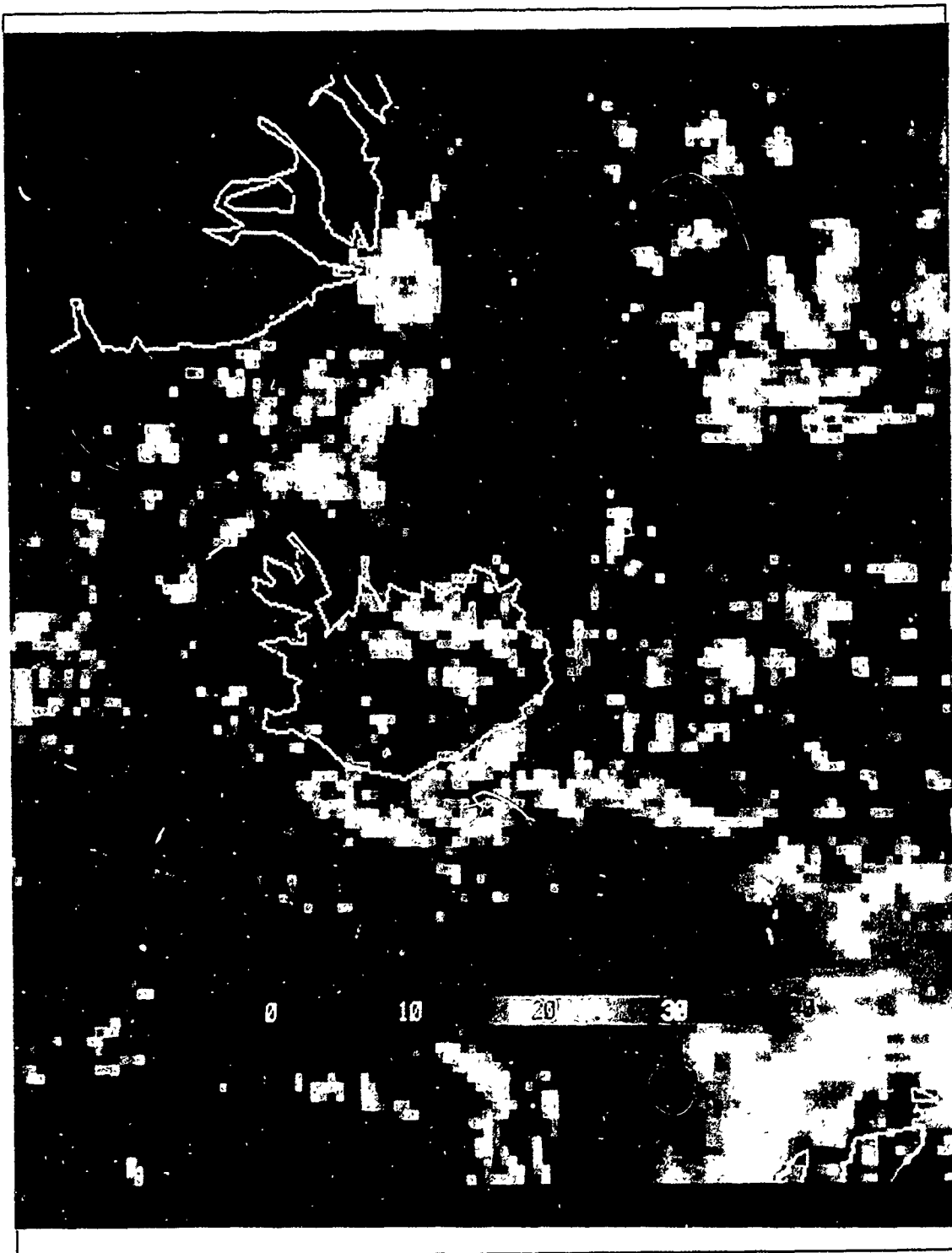


Fig. 27. LOW3 composite for June 1984.

20-25%, whereas in 1984 the same region shows values near 15% (light blue/green). To the east-southeast of Iceland, 1984 values are approximately 10% higher (green/yellow versus light blue/green). This bright "plume" also seems consistent with terrestrial sources due to the prevailing northwest winds during June 1984.

Two important inferred-DMS source regions appear to be related to changes in cloud reflectance between the two years. The small $1 \mu\text{mol/L}$ silicon anomaly to the north of Iceland in June 1982 (Fig. 6) is the only silicon anomaly present near Iceland for this timeframe. The inferred-DMS source is associated with the bright feature (20% reflectance) in the LOW3 image. The region of largest differences between June 1982 and June 1984 are to the north-northwest of Iceland in the Denmark Strait. These higher values in June 1984 are in the vicinity of the inferred-DMS source region, and this brighter region seems to actually map out the same two-pronged silicon anomaly shape given by Fig. 5. Here the LOW3 values for June 1984 are between 15-20% (green/yellow), and the June 1982 values are between 5-10% (light blue).

D. SECTOR RESULTS

Composite data from June 1982 and June 1984 were additionally resolved into eight sectors around Iceland. These sectors are shown in Fig. 28. The sectors were chosen based on surface wind analyses as well as DMS-source region information. As indicated earlier, the overall surface wind analyses show light winds during both data collection periods, with wind directions varying from northwest to east. Based on these observations, the cloud response should appear in the vicinity of the DMS source region. Table 1 shows the LOW1 and LOW3 reflectance values for both years according to sector. For both the LOW1 and LOW3 sector averages, the general trend is that southwest of Iceland (sector 1) the June 1982 values are slightly higher, but, moving clockwise around the island, the June 1984 reflectance values are greater. One trend warranting further investigation is that with the exception of sector 3 (NW), all sector's LOW1 and LOW3 values exhibit a similar trend from June 1982 to June 1984. For example, in sector 6 the LOW1 and LOW3 values in June 1984 are both greater than the LOW1 and LOW3 values in June 1982. This is consistent with the dependence of channel 1 reflectance on size distribution and indicates that this dependence is significant.

Table 1. COMPARISONS OF LOW1 AND LOW3 REFLECTANCE VALUES BY SECTOR, for June 1982 and June 1984.

Sector	1982 LOW1	1984 LOW1	1982 LOW3	1984 LOW3
1-SW	53.0	43.5	15.9	12.7
2-W	54.8	46.5	14.9	13.3
3-NW	65.6	54.3	9.2	14.2
4-N	48.5	52.4	9.2	16.3
5-NE	40.5	42.0	10.6	10.8
6-E	40.1	45.7	12.4	13.8
7-SE	52.7	64.8	12.9	16.1
8-S	58.6	60.0	13.9	15.5

For the LOW1 comparisons, the western sectors (1-3) show higher values in June 1982 than in June 1984. Sectors 4-8 indicate higher values in June 1984. For the LOW3 comparisons, sectors 1 and 2 indicate slightly higher reflectances in June 1982. However, sectors 3-8 show higher June 1984 reflectances. Of particular note is sector 4 to the north, where June 1984 values are nearly 80% greater than in June 1982. This is the location of the maximum silicon anomaly of greater than 4 $\mu\text{mol/L}$. Again, this suggests that inferred- DMS sources are correlated with higher channel 3 reflectance values.

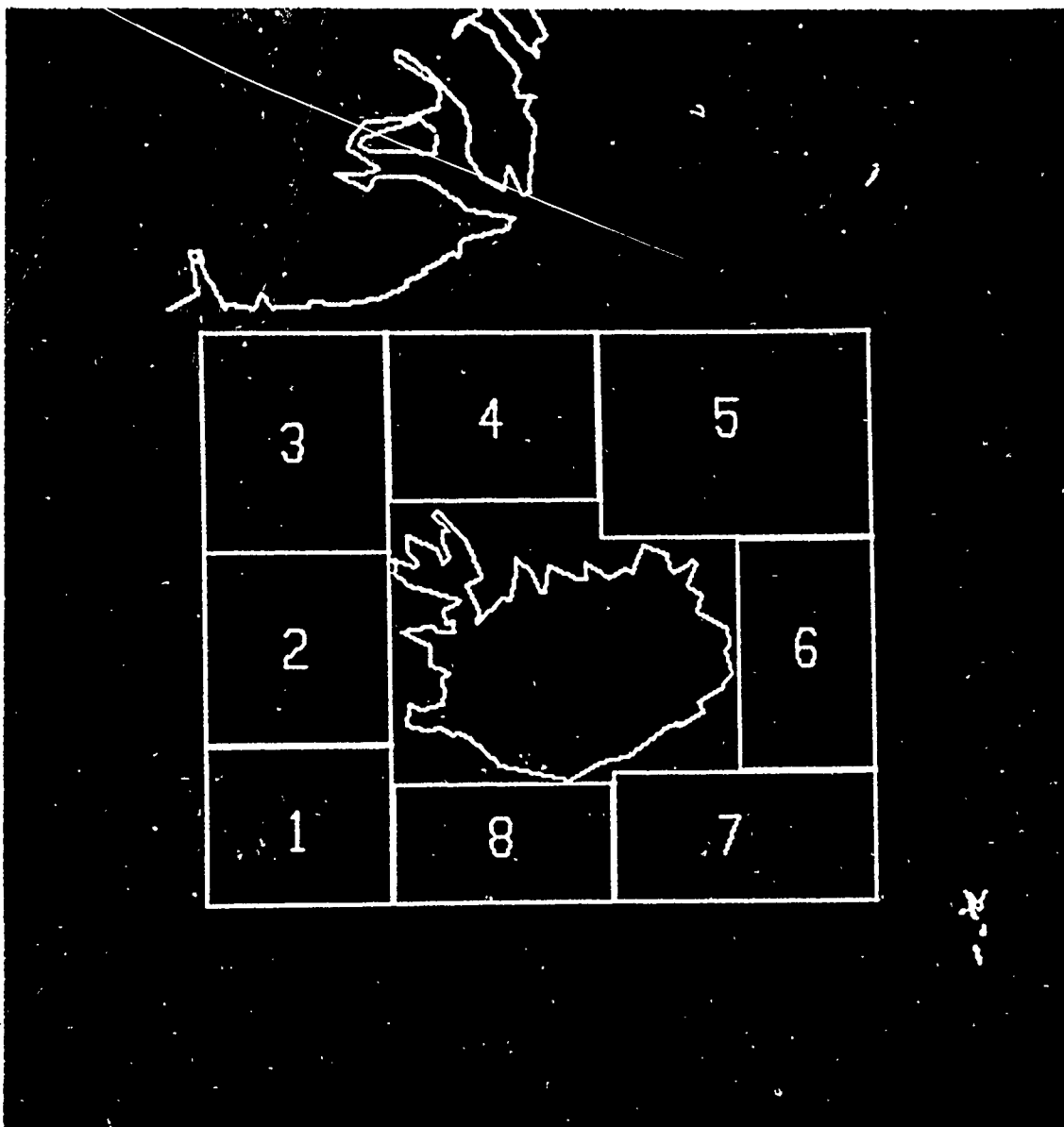


Fig. 28. Location of the eight sectors around Iceland.

IV. CONCLUSIONS AND RECOMMENDATIONS

A. CONCLUSIONS

This study used silicon anomaly information in the Denmark Strait to infer dimethylsulfide (DMS) source regions. It was assumed that these DMS source regions created new CCN via $\text{NSS} - \text{SO}_4^{2-}$ particles. Variations in cloud reflectance were expected due to changes in size distribution of the cloud droplets. Measurements were made using the AVHRR sensor from the NOAA-7 satellite. Basic radiative theory indicates that channel 1 reflectance at $.63 \mu\text{m}$ is not a decisive indicator of size distribution due to the combined effects of cloud thickness, LWC and this size distribution. However, channel 3 reflectance has a clear dependence primarily on the size distribution due to moderate absorption at a wavelength of $3.7 \mu\text{m}$. Channel 1, 3 and 4 images were processed for each of the nine days in June 1982 and the seven days in June 1984. Then composites were produced for channel 1 and channel 3 data by averaging pixel values after invoking criteria to eliminate cloud-free and high cloud areas. The results presented were significant although the data sets were limited and quantitative correlation between cloud reflectance and inferred-DMS sources is not possible.

As expected, the LOW1 composites reveal differences in reflectance values between the two years, but no conclusive results could be drawn relating channel 1 reflectance to DMS sources due to the dependence of reflectance on size distribution as well as LWC and cloud thickness. The LOW3 composites, on the other hand, reveal more interesting and more significant results. The most significant variation in LOW3 reflectances between the two years occurred to the north-northwest of Iceland. The $4 \mu\text{mol/L}$ silicon anomaly coincided with an approximate 80% increase in LOW3 reflectance values in the June 1984 case. A $1 \mu\text{mol/L}$ silicon anomaly in June 1982 correlated with a significant bright region (20%) in LOW3 reflectance values. Based on these results, the inferred-DMS source regions are consistent with higher relative channel 3 reflectance values. In addition, brighter values in June 1982 to the southwest of Iceland were attributed to land sources due to the prevailing winds as well as coherent brightness features over the land and sea. A similar conclusion was drawn in June 1984 with the brighter region to the southeast of Iceland.

B. RECOMMENDATIONS

Although the results in this study were consistent with the expected outcomes for the limited data set, the following recommendations are made. First, the DMS sources used here were inferred from silicon anomaly information. A more direct link would be to study variations in cloud reflectance in areas where actual DMS data are available. In either case, more "bloom" versus "non-bloom" cases need to be studied to allow more quantitative statistical correlations to be made. This is especially true for channel 1 reflectance due to the dependence on the three varying quantities. These studies also should be extended to investigate other DMS source regions outside the Denmark Strait. Finally, the various processes within the Charlson feedback loop that are not fully understood need to be examined to better define the effects of DMS sources on cloud reflectance characteristics.

LIST OF REFERENCES

- Allen, R.C., Jr., 1987: Automated satellite cloud analysis: A multispectral approach to the problem of snow/cloud discrimination. M.S. Thesis, Naval Postgraduate School, Monterey, CA, 113 pp.
- Charlson, R.J., J.E. Lovelock, M.O. Andreae, and S.G. Warren, 1987: Oceanic phytoplankton, atmospheric sulphur, cloud albedo and climate. *Nature*, **326**, 655-661.
- Coakley, J.A., Jr., R.L. Bernstein, and P.A. Durkee, 1987: Effect of ship-track effluents on cloud reflectivity. *Science*, **237**, 1020-1022.
- Coakley, J.A., Jr., and R. Davies, 1986: The effect of cloud sides on reflected solar radiation as deduced from satellite observations. *J. Atmos. Sci.*, **43**, 1025-1035.
- Hunt, G.E., 1972: Radiative properties of terrestrial clouds at visible and infra-red thermal window wavelengths. *Quart. J.R. Met. Soc.*, **99**, 346-369.
- Kidwell, K.B., 1986. *NOAA Polar Orbiter Users Guide*. National Environmental Satellite Data and Information Service, Washington, D.C., 120 pp.
- Lauritson, L., G.J. Nelson and F.W. Porto, 1979: Data Extraction and Calibration of TIROS-N/NOAA radiometers. NOAA Technical Memorandum NESS 107, U.S. Dept. of Commerce, Washington, D.C., Appendix B.
- Liou, K.N., 1980: *An Introduction to Atmospheric Radiation*. Academic Press, New York, 392 pp.
- Mineart, G.M., 1988: Multispectral satellite analysis of marine stratocumulus cloud microphysics. M.S. Thesis, Naval Postgraduate School, Monterey, CA., 138 pp.
- Pruppacher, H.R., and J.D. Klett, 1978: *Microphysics of Clouds and Precipitation*. Reidel, Dordrecht, 398 pp.
- Taylor, V.R. and L.L. Stowe, 1984: Reflectance characteristics of uniform earth and cloud surfaces derived from NIMBUS-7 ERB. *J. Geophys. Res.*, **89**, 4987-4996.
- Twomey, S., 1977: The influence of pollution on the shortwave albedo of clouds. *J. Atmos. Sci.*, **34**, 1149-1152.
- Twomey, S.A., M. Piepgrass and T.L. Wolfe, 1984: An assessment of the impact of pollution on global cloud albedo. *Tellus.*, **36B**, 356-366.

INITIAL DISTRIBUTION LIST

	No. Copies
1. Defense Technical Information Center Cameron Station Alexandria, VA 22304-6145	2
2. Library, Code 0142 Naval Postgraduate School Monterey, CA 93943-5002	2
3. LT Greg A. Eisman, USN NOCC/JTWC COMNAVMARIANAS Box 12 Facility FPO San Fransisico 96630-2926	1
4. Robert J. Charlson Dept. of Atmospheric Sciences, AK-40 University of Washington Seattle, WA 98195	1
5. Dr. Jon Olafsson Marine Research Institute Skulgata 4, PO Box 390 Reykjavik, Iceland	1